Switching Notes
Note 4
June 1967

Laser-Triggered Megavolt Switching

Lt Jerry Ray Bettis
Air Force Institute of Technology
and
Air Force Weapons Laboratory

Abstract

A focused, Q-spoiled laser, aligned along the interelectrode axis of a charged spark gap, was used to induce dielectric breakdown of the gap. The effect of the following parameters on the triggering delay was studied: gap polarity, reduced field in the gap, percentage of the self breakdown voltage to which the gap was charged, pressure of the gas dielectric (620-21,000 torr), laser power (75-300 MW), and gap spacing (0.75-3.0 cm). Delay times as short as two nsec, with jitter less than one nsec, were recorded. Self breakdown voltages varied from 30 kV to 1.5 MV. Good agreement was found between the observed results and results predicted from the streamer theory of gas breakdown.

Preface

This report covers a six-month research program which I conducted at the Air Force Weapons Laboratory, Albuquerque, New Mexico, in cooperation with the Air Force Institute of Technology. The research was concerned with the determination of the trigger delay and switch jitter of a laser-triggered spark gap. Additionally, we wanted to demonstrate that a laser-triggered spark gap could electrically switch megavolt systems. Finally, we wanted to begin a theoretical study of the breakdown mechanism.

I was initially motivated toward the project by Dr. Leno Pedrotti, AFIT Physics Department Head, whose interest in the project convinced me of its importance. I am also convinced that it should not be many years until laser technology has progressed to the point that a switch such as the one described here will be a practical method for switching high power systems. However, if my rose-colored glasses should turn gray, I will at least have had the opportunity to work with a man of Dr. Arthur Guenther's caliber.

I now wish to take this opportunity to thank those people who were most liberal in the assistance they gave me.

I suppose that if a man were to have been fortunate enough to work for Niels Bohr, he would have thanked him for "inventing" the atom. It is with the same gratitude that I thank Dr. Guenther for not only inventing laser-triggered spark gap switching, but for having the ability and willingness to solve the many engineering problems which developed during my research period. One should always feel fortunate to work in a lab where the supervisor has graduated from the lab and understands the problems associated with basic research. My indebtedness was also incurred by Dr. Raymond V. Wick, postdoctoral fellow, who helped me keep the laser operating, and by Ellis Dawson, who nearly made an electronics technician out of me. I also gratefully acknowledge the assistance of: Leonie Boehmer, who helped me prepare the drawings and graphs, S/Sgt. Jerry Teale and John Hebenstreit, whose rapid machine shop labors kept the project from faltering, and Willie Kunzler, who helped me reduce the data. Finally, I would like to thank Beverly Bettis, who not only ran our household and supervised our noisy children, but also corrected my grammar and typed the final manuscript.

Jerry R. Bettis

Contents

Contents

List of Figures

Figure Page

List of Important Symbols

V_{SB} = Self Breakdown Voltage of the Spark Gap

V_{CH} = Ug = Potential Between Electrodes

$\%V_{SB} = V_{CH}/V_{SB} \times 100\%$

Δt_d = Time Delay Between the Arrival of the Laser Pulse at the Gap and the Complete Breakdown of the Gap.

α = First Townsend Coefficient

j = Jitter or Standard Deviation of Δt_d

p = Pressure of the Gas Dielectric

d = Axial Distance Between Electrode Surfaces

L_s = Inductance of the Switch

V_e = Electron Drift Velocity

V_+ = Drift Velocity of Positive Ions

E/p = Reduced Electric Field in the Gap

$\mathcal{E}$ = Energy

M = Laser Power

LASER-TRIGGERED MEGAVOLT SWITCHING

I. Introduction

Statement of the Problem

This study was an attempt to develop an electrical switch which would: (1) hold off potential differences in the megavolt range, (2) have a dynamic impedance of less than one ohm and exhibit inductance in the nanohenry range, and (3) completely close with the rise time of the current less than five nanoseconds, with switch jitter less than one nanosecond. Switch jitter may be defined as the variation in the time between a given reference event and the complete closure of the switch. In addition to these constraints, it may be necessary to require nanosecond variation in the time between a given command signal and the complete closure of the switch--which is termed command jitter. Existing electrical switches fail to meet these stringent requirements. However, from the time that A. H. Guenther and A. D. Griffin of the Air Force Weapons Laboratory demonstrated that a focused Q-spoiled laser pulse could be used

to break down a charged air gap, it has been evident that laser-triggered spark gap switching could probably meet these requirements. This investigation was an extension of the initial study by Pendleton and Guenther (Ref. 17).

Specifically, this study involved the precise determination of the delay between the arrival of the laser pulse at the gap and the complete breakdown of the gap. The complete breakdown was defined as being coincident in time with the rise time of the complete discharge. The delay between the arrival of the laser pulse and the complete breakdown of the gap (termed trigger delay) and the switch jitter were measured as a function of the polarity of the gap, of the pressure of the gas dielectric, of the dielectric composition, and of the percent of self-breakdown voltage to which the gap was charged. In the study of the feasibility of laser-triggered spark gap switching, extension to the megavolt range was required, and in the final portion of the research period the requirement was met.

Importance of the Problem

Electrical switches with the requirements listed at the beginning of this paper are necessary to switch various electrical systems such as high-energy field-reversal generators and other pulse power sources useful for the

simulation of nuclear detonation effects and phenomena. In particular, the requirements for high-voltage holdoff and rapid-current risetimes are set by simulation devices, while the requirement for low jitter is set by such devices as the Blumlein generator which requires a high degree of synchronization in several switches that are triggered by a common signal. Low jitter may also be required in particular arrangements of devices used for weapons simulation. An example of the problems associated with the study of the effects of nuclear weapons may help the reader to place the proper emphasis on the study of laser-triggered spark gap switching.

Since the United States entered into the Limited Test Ban Treaty, which prohibits the detonation of nuclear devices in the atmosphere, in space, and underwater, weapons simulation has grown in importance. This is because not all the problems in the study of the effects of nuclear detonations are amenable to underground testing. As an example, the times of flight of various radiation outputs are similar, and it is very difficult to sort out effects produced by the different output characteristics of nuclear weapons. Thus, it has become a requirement to produce a controlled explosion in the laboratory.

Weapons simulation in the laboratory requires the release of an enormous amount of energy in a very short time (high power). Furthermore, an environment similar to that produced by a nuclear detonation must be produced to be of practical benefit. That is, weapons experts demand high radiation levels of an appropriate character for irradiation of a high uniformity throughout the largest possible volume. To produce such an environment, peak powers greater than 10^{12} watts must be achieved in times less than 100 nanoseconds. It is not a simple process to build a machine with these capabilities.

Devices used to simulate nuclear detonations consist primarily of an energy storage system, a switching mechanism, and some type of transducer which converts the stored energy into the desired output. It is the combination of these separate entities into a single machine which makes the task of building a weapons simulator so difficult. Associated with any transducer is an inherent inductance, L. The energy storage system has associated with it a capacitance, C; and the switch has a resistance, R, and inductance, L_S, associated with it. The pulse duration of the release of the energy is proportional to $\sqrt{LC}$, if $L_S < L$, thus, C must be made very small to get times of the order of those characteristic of weapon outputs. However, the stored energy is $E = 1/2\ CV^2$,

thus, very high voltages are necessary to satisfy the energy (or power) requirements. At these high voltages (>10MV) field emission processes are dominant. Since field emission transducers will unavoidably produce copious quantities of electrons, the conversion from stored energy to high energy electrons is then maximized, and the electrons are later transformed into weapon-like radiations. As previously mentioned, energy storage systems with greater than 10^{12} watts capacity are necessary in weapons simulation, due primarily to the inefficiencies associated with the desired radiation production processes as outlined above.

Systems such as the one just considered, in which R, L, and C exist in discreet sections, are feasible when the times of energy deposition are in the radio frequency range. For pulse durations less than 100 nsec, it is necessary to build the system such that R, L, and C are distributed throughout (e.g. a coaxial transmission line geometry). In such transmission line geometries the pulse duration is determined by the length of the line, and L becomes more important in pulse risetimes than in pulse durations.

For a hypothetical 10^{14} watt system which is operated at 10^7 volts, the characteristic impedance becomes $R=1\Omega$. Since the risetime of the pulse is proportional to L/R, L must be made very small since $R\approx1\Omega$. But to operate at

10^7 volts, large separations, which are needed for insulation, increase L (particularly L_s). To reduce L_s, n switches could be used to trigger the system since $L_s(\text{total}) = L_s/n$. But in order to keep the same pulse risetime as a single switch of inductance, L/n, the n switches must close simultaneously to within an order of magnitude less than the desired risetime. Thus, the reproducibility of the trigger delay (switch jitter) must be very good for the n switches to trigger the system in the desired time interval.

The switch must have a very low impedance, for if the system has $R = 1\Omega$, and the switch has $R_s = 1/2\Omega$, fully half the energy is dropped in the switch. Furthermore, the switch must close very shortly after a triggering signal arrives, since a perturbation of the switch which initiates switch closure also initiates the beginning of the deposition of the energy, thus, increasing the risetime. Finally, it appears impossible to construct a single machine with a 10^{14} watt capability anywhere but on site. Ion Physics Corporation is currently building a 10 MV-10^{12} watt system which incorporates the largest sized pressure vessel transportable by rail. It is then proposed to couple several high-wattage systems to a common transducer and fire all the systems simultaneously with a common triggering signal. This places an even higher premium on low switch jitter, for

if all the systems did not fire simultaneously, reflected waves due to impedance mismatching could cause serious mechanical and electrical imbalances as well as degradation of the system performance.

From such considerations as these come the switch requirements listed at the beginning of the introduction.

Survey of Previous Papers

The initial paper on laser-triggered spark gaps was published by Pendleton and Guenther (Ref. 17) in November, 1965. A laser was focused in the gap from an angle of incidence perpendicular to the inter-electrode axis (see Fig. 4 for arrangement used in the present study). They reported triggering delays as short as 10 nsec. They also reported the variation in the delay as a function of the pressure of the dielectric gas, of the percent self-breakdown voltage to which the gap was charged, and of the distance of focus from the electrode. They concluded that short delay times favor high gas pressure, high percent self-breakdown voltage, and small focal point distances from the electrodes.

A study by Gilmour, Bliss, and Clark (Ref. 8) reported on a vacuum-gap triggering system. They reported triggering delays in the microsecond range and the variation in the delay as a function of the target electrode material. They

concluded that the delay increases with increasing atomic weight of the electrode material.

A recent document (published since the consumation of this report) by Dr. F. Deutsch (Ref. 6) of Cern reports on a feasibility study of a laser-triggered spark gap. In this study a delay line was discharged by a spark gap of coaxial design into a terminating resistor. A Q-spoiled laser with 20 nsec pulse width and up to 50 MW power was used. Gap lengths varied from three to eight mm and voltages up to 85 kV were reached. Formative times of down to one nsec and jitters below one nsec were found. It was reported that it made no difference whether the target electrode was charged positive or negative. The prime differences in his report and the present study are related to variations due to much smaller gap spacing, lower laser power, and the lower peak operating voltage.

The final paper which the author found in his search of the literature was a study by Barbini (Ref. 2) which reported only on the phenomenological aspect of coaxial triggering, and it contained no delay or jitter measurements.

II. Theory

Introduction

It will be instructive to review some of the basic principles of the electrical breakdown of gas dielectrics which have a bearing on the experimental observations. The author does not imply that the theory contained in this section conclusively explains the observed behavior, but on the basis of this theory, the observed dependence of trigger delay times on gap polarity, ground connection, reduced field, and laser power is not unexpected. These dependencies are, in the main, qualitative only because the mathematical model of the breakdown mechanism is nebulus and open to some debate. Due to the primarily experimental nature of this study, a complete theory on gas-filled spark gap breakdown is not attempted, but the reader is directed to such sources as von Engle (Ref. 22), Meek and Craggs (Ref. 15), and the highly readable book by Raether (Ref. 19). Finally, in section VI, observed and theoretically predicted behaviours are compared.

Conditions

To adapt existing theories of the breakdown mechanism of gas-filled spark gaps to laser-triggered spark gap breakdown, it is necessary to state the following conditions:

(1) the laser beam can produce ionization in the gas for the pulse duration, whether or not visible recombination radiation is observed (Ref, 18:499-508), (2) this ionized path which forms along the laser beam collapses very quickly after the laser pulse ends, and (3) laser impingement on a material surface is followed very closely by electron and ion emission (Ref. 7:4965). A more complete discussion of the interaction of laser beams with matter is included later in this section.

Growth of Ionization

The theory presented here is for the normal gas breakdown of a gap with initial ionization due to ultra-violet photoelectric emission or gas ionizing radiation such as α-particles. However, since the theory is basic in nature, its application can be considered in terms of laser-induced breakdown processes.

If N_o electrons per second are produced at the cathode of a charged spark gap, and each electron makes α ionizing collisions per cm of travel, then the rate of production of ion pairs in a length dx is

$$dN = N_x \alpha dx \qquad (1)$$

where N_x is the number of electrons at x. By integrating

from x = o to x = d, we obtain the number of electrons, N, at d as

$$N = N_o \exp(\alpha d) \tag{2}$$

If instead of producing electrons at the cathode, we shield the electrodes and produce ion pairs throughout the volume, then each electron starting a distance x from the anode will be multiplied to $\exp(\alpha x)$ at the anode. Production of $N_i dx$ electrons over each length dx in the gap gives the number n, which arrives at the anode per cm^2 per sec as

$$n = \int_o^d N_i \exp(\alpha x)\, dx$$

or

$$n = (N_i/\alpha)\left[\exp(\alpha d)\right] - N_i/\alpha \quad \text{(Ref. 22:174)} \tag{3}$$

For processes which produce both uniform ionization in the gap and emission from the cathode, the total number flux, N_T, which arrives at the anode is

$$N_T = N_o \exp(\alpha d) + (N_i/\alpha)\left[\exp(\alpha d) - 1\right]$$

or

$$N_T = (N_o + N_i/\alpha)\exp(\alpha d) - (N_i/\alpha) \tag{4}$$

From Eq (4) it is seen that the multiplication of current carriers is strongly dependent on α. In the classical theory of breakdown, α is called the first Townsend coefficient. It will be seen later that α/p is strongly dependent on the reduced field, E/p, where E is the electric

field in the gap, and p is the gas pressure.

Such processes as were just described are given the name electron avalanche. It is this type of phenomenon which gives the name to the Avalanche or Townsend breakdown mechanism.

Townsend-Avalanche Mechanism

Physically an electron avalanche proceeds as a conical-shaped growth of ionization. The electron cloud at the front of the avalanche spreads out, due to diffusion, as the avalanche grows. The positive ions are nearly stationary, compared to the electrons, since $v_e \geq 100 v_+$, where V_e and V_+ are the drift velocities of the electrons and positive ions, respectively. The conical shape of the avalanche, then, is due to the spreading path of ion pair production and the relatively stationary positive ions left behind.

During the avalanche process copious quantities of ionizing photons can be produced. When ionizing collisions occur, energy is given off in the form of light quanta. If the amplification of the avalanche is increased (e.g. by increasing the electric field in the gap or the number of initial electrons), the number of positive ions and emitted photons increases, thereby increasing the probability that new electrons are liberated from the cathode or dielectric

volume. These secondary electrons produce new avalanches in the next generation (Ref. 19:90). This process continues until the current in the gap increases to a point of instability and breakdown follows.

Each avalanche has associated with it a region of high field intensification caused by the ion space charge. It is this space charge of the slow positive ions produced by the rapidly succeeding avalanches which produces the rapid current growth (Ref. 20:113). According to Raether, the current form of an avalanche breakdown will consist of a rapid current caused by the primary electrons followed by an exponential increase which leads to breakdown. In the streamer mechanism (to be described later), which is more than 100 times as rapid as the avalanche, it is the effect of the space charge of the avalanche on its own development which transforms it into a plasma streamer of high conductivity (Ref. 19:113).

Because of the short times involved in laser-triggered spark gap breakdown, the streamer mechanism is probably more applicable and will be considered now.

Streamer Mechanism

Streamer breakdown occurs as an outgrowth of a normal avalanche. The avalanche progresses in the normal manner

until the amplification reaches a certain critical value. The critical parameter is the number of charge carriers in the head of the avalanche. For a single primary electron the number is simply

$$N_{crit} = exp(\alpha x_{crit}) \tag{5}$$

where X_{crit} is the distance the avalanche progresses before it is transformed into a plasma streamer. For N_o primary electrons the number at X'_{crit} is

$$N_{crit} = N_o exp(\alpha x'_{crit}) \tag{6}$$

where $x'_{crit} < x_{crit}$. Thus, it is evident that the time it takes to initiate a streamer is shortened if the number of initiating electrons is increased, since the distance of travel of the avalanche is shorter. In a like manner, the time for initiating a streamer is shortened if α is increased. These two facts will prove to be necessary in explaining the observed delay time dependencies.

Raether states that the streamer mechanism is favored in long gaps with $pd \gtrsim 1000$ cm-torr because sufficient amplification will not occur in a small gap to cause streamer formation. He modifies this to mean that the number of charge carriers in the avalanche must reach a certain value before streamers can form. Thus, it is seen that gaps with

$pd < 1000$ cm-torr can undergo streamer breakdown if the number of initial electrons, N_o, is large enough (Ref. 1-1003).

It is the space charge associated with the large number of charge carriers which determines when streamer formation will occur. Raether calculates breakdown voltages on the assumption that streamers form when the space charge field,

$$E_r = 1.5 \times 10^{-7} \epsilon \times p(\alpha d)/r_d^2 \qquad \text{(Ref. 19:78)} \qquad (7)$$

where r_d is the radius of the head of the avalanche, is equal to the applied field E_o. The effect of the space charge on the applied field will now be considered.

The space charge effect of an avalanche is represented schematically in Fig. 1. The dotted lines in Fig. 1 indicate

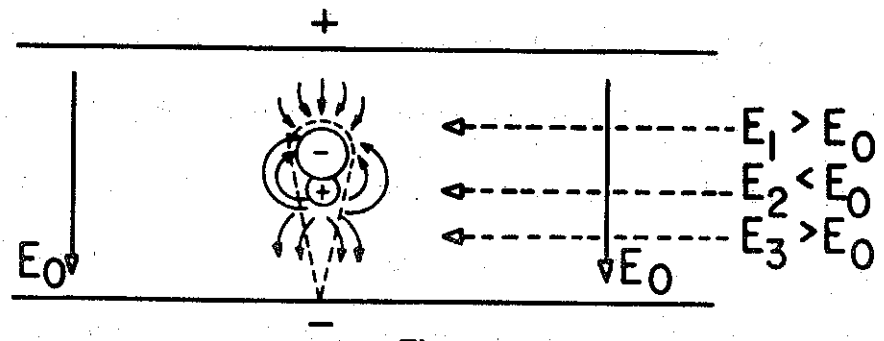

Fig. 1

THE EFFECT OF SPACE CHARGES OF AN AVALANCHE OF HIGH MULTIPLICATION ON THE ELECTRIC FIELD E_0 (REF 22/79)

the outline of the avalanche as recorded in cloud chamber photographs. Here E_1, E_2, and E_3 are the net fields in the

vicinity of the avalanche. From Fig. 1, the increased field on the anode side of the streamer partially accounts for the very rapid movement of the streamer. The streamer velocity of 8×10^7 cm/sec is considerably greater than the drift velocity of electrons under the influence of the same electric field $(v_e \approx 1.0 \times 10^7 \text{cm/sec})$.

It is interesting to note that streamers directed toward the cathode have greater velocities than anode directed streamers. Meek and Craggs give the values of 8×10^7 cm/sec and 2×10^8 cm/sec for anode and cathode directed streamers, respectively (Ref. 15:181). Raether explains this phenomenon by considering the production of gas ionizing radiation. It should be noted here that this explanation also proves valid for the propagation velocities of the cathode and anode directed avalanches. That is, the propagation velocity of a cathode directed avalanche should be greater than the propagation velocity of an anode directed avalanche. Then, if the same number N_o of ion pairs are produced at both the cathode and anode (Ref. 7:4963),

$$N_{crit} = N_o^+ \exp(\alpha x_{crit}^+) \tag{8}$$

and

$$N_{crit} = N_o^- \exp(\alpha x_{crit}^-) \tag{9}$$

where N_o^+ and X_{crit}^+ refer to the anode as the emitting electrode, and N_o^- and X_{crit}^- refer to the cathode as the emitting electrode. Now N_{crit} is nearly constant and $N_o^+ = N_o^-$. Thus, $X_{crit}^+ = X_{crit}^-$, but since the cathode directed avalanche propagates faster, the time to reach critical amplification is shorter. Thus, one should expect that using the anode as the target electrode would result in shorter delay times when X_{crit} is significant.

Figure 2 shows qualitatively the importance of the gas ionizing radiation. It is seen that electrons formed in front of the anode directed streamer (avalanche) are drawn quickly to the anode by the increased space charge field (Fig. 1).

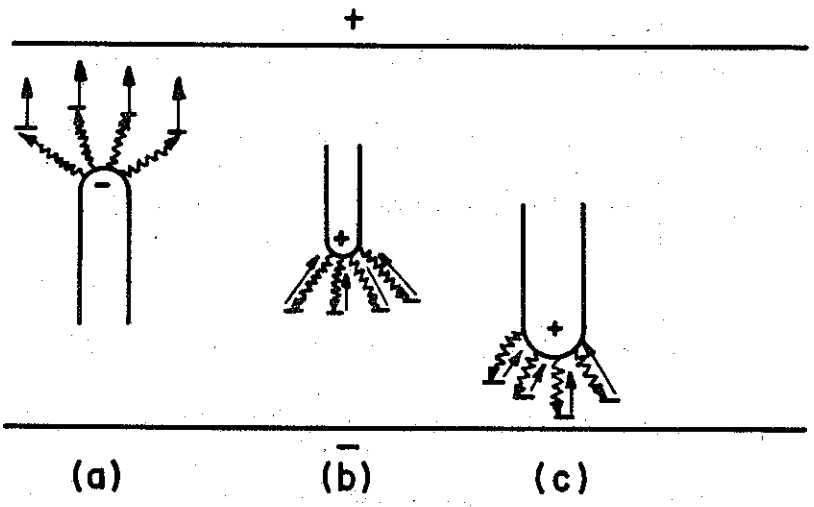

Fig. 2

DEVELOPMENT OF THE STREAMERS BY GAS IONIZING RADIATION (REF 22/127)

Only a small percentage of electrons help propagate the bulk of the avalanche. Conversely, electrons which are produced in front of the cathode directed streamer are immediately drawn into the head of the avalanche, creating more ionization, thereby rapidly propagating the streamer toward the cathode. A criterion for the formation of a streamer from an avalanche will now be given.

Condition for Streamer Breakdown

Breakdown criteria for the streamer mechanism have been advanced independently by Meek and by Raether. The dependence of the formative time lag, or the time from initial electron emission to complete breakdown, on the reduced field, E/p, can be determined from these criteria. The formative time lag has been the subject of a calculation by Fletcher (Ref. 15:275), which gives a dependence on E/p that is in agreement with the dependencies found by Meek and Raether.

It should be noted here that in previous studies of gap breakdown, both statistical and formative time lags were considered. The statistical time lag deals with the time it takes for an initial charged particle to be freed from the electrode. In laser-initiated breakdown, electrons and ions are produced in abundance without delay, thus, the statistical

time lag vanishes. The formative time lag is the time required for a conducting channel (spark) to bridge the gap. This formative time lag is no smaller than the trigger delay time in the study of laser-triggered spark gap breakdown.

The empirical condition for streamer formation is

$$\alpha x_{crit} \approx 20 \tag{10}$$

If the streamer theory of gas breakdown is applicable to laser-triggered spark gap breakdown, the theory presented here should allow one to predict the temporal behavior of the breakdown.

Application of Streamer Theory to Laser-Initiated Breakdown

The delay time between the arrival of the laser pulse (coincident with initial charged particle production) and the complete gap closure should correspond to the time required for the avalanche to reach the critical amplification value

$$\exp(\alpha x_{crit}) \cong 4 \times 10^8 \tag{11}$$

Then, for $x_{crit} = V\Delta t_d$, where V is the rate of propagation of the avalanche and Δt_d is the time delay from carrier initiation to breakdown,

$$V\alpha\Delta t_d = \ln(4 \times 10^8) - \ln N_o$$

or $$\Delta t_d = \frac{20 - \ln N_o}{\alpha v} \qquad (12)$$

Since we have been looking for gross dependencies, the propagation time of the streamer has been neglected. This propagation time will have the effect of increasing Δt_d as the gap spacing, d, is increased, so that Eq (12) should more properly read

$$\Delta t_d = \frac{20 - \ln N_o}{\alpha v} + \frac{d - x_{crit}}{s} \qquad (13)$$

where S is the streamer velocity. For the same initial carrier production, N_o, $\Delta t_d(E/p)$ should vary inversely with $v(E/p) \cdot \alpha(E/p)$. Raether gives

$$v_- = (0.244)(E)^{1/2} \text{ cm/sec} \qquad \text{(Ref. 15:278)} \qquad (14)$$

as the avalanche formation velocity of an anode directed avalanche. However, from values of α in air found by Sanders (Ref. 15:62)

$$\alpha = A(E/p)^{9.2}, \quad 20 \leq E/p \leq 36 \text{ V/cm-torr} \qquad (15)$$

Therefore, the variation in v_- is insignificant for qualitative comparisons. On the basis of Eq (12) a plot of $\ln(\Delta t_d)$ vs $\ln(E/p)$ should have a slope ≈ -9. This value will be compared in section VI with experimental observations.

Incorporated in the constant A of Eq (15) was the pressure; so that if A = Bp, Eq (15) would read

$$\alpha/p = B(E/p)^{9.2} \tag{16}$$

Thus, for E/p = constant, an increase in p will increase α. Then, since Δt_d is inversely proportional to α (Eq (12)), Δt_d should decrease with increasing pressure at constant E/p. This dependence was observed by Pendleton and Guenther (Ref. 17:1549). At a reduced field of E/p = 43 volts/cm-torr, the empirical curve of $\Delta t_d = C + (8.5 \times 10^4)(1/p)$, where C is a constant, fit the data for $200 \text{ torr} \leq p \leq 614 \text{ torr}$ within 3%.

In Meek and Craggs (Ref. 15:210) the formative time lag was investigated as a function of external gas ionizing radiation. That is, an external source of radiation was placed near the spark gap so that the gas was partially ionized. Charged particles were then liberated from an electrode, and the resulting formative time lag was studied as a function of the intensity of the external radiation source. It was found that for the greatest intensity of radiation used there was no appreciable scatter in formative time lags (i.e. low jitter), but as the intensity was decreased, the scatter (jitter) increased. This is because the statistical time lag, that is the time it takes to

produce the first charge carriers in the gap, is reduced as the external radiation intensity is increased. Thus, one should expect low values of jitter whenever breakdown occurs during the duration of the laser pulse. Then as the laser pulse dies away, the rate of production of ion pairs in the dielectric volume decreases and jitter should increase slightly for breakdown times near the end of the laser pulse duration. Jitter should then increase faster for breakdown times which occur an increasing time after the laser pulse has ended. Since this variation of the jitter has been observed (see section VI), it lends credence to the condition stated earlier that the ionized path formed by the laser collapses quickly after the laser pulse ends.

Since, as has been stated, avalanche propagation velocities and streamer velocities are greater toward the cathode, and unless there is a marked difference in the emission from the cathode compared to the anode, shorter delay times should result when the target electrode is the anode.

The effect of keeping one electrode at ground potential while charging the other was investigated by Cobine. He states, "The effect of bringing the ground potential up to the gap is to increase the electrostatic field of the ungrounded sphere." (Ref. 4:172) Since $\alpha/p = B(E/p)^{9.2}$,

the multiplication factor is increased near the charged electrode. Furthermore, the increased field near the charged electrode will increase V_- . These effects should manifest themselves in shorter delay times when the charged electrode is the target electrode.

Finally, since Δt_d depends on the time required to create a sufficient number of charge carriers in the avalanche, an increase in the power of the laser pulse (thereby creating more charge carriers) should decrease Δt_d . This should be most evident at low E/p values where α is correspondingly low. This effect was noted by Pendleton and Guenther (Ref. 17:1548) for low laser powers. However, above a certain value of the power the dependence was nil. This may be attributable to the fact that the laser was focused in the gap. At a certain laser power all the particles in the focal volume of the laser will be ionized, and further increase in the power will only produce ion pairs in the path of the laser beam and no more in the focal volume. In the present study the laser was focused on the electrode and it traversed the path of the spark channel. Thus, much higher power than 80 MW (Pendleton's maximum laser power) would be needed to saturate ion pair production; then the dependence of Δt_d on laser power should hold to much higher powers than previously reported.

Current Forms in the Gap

The condition which was set earlier concerning the fast closure of the laser-induced ionized gas is further substantiated by the current forms viewed in the breakdown process. In the following discussion, $\%V_{SB}$ will be defined as that percent of the static breakdown voltage to which the gap is charged.

According the Raether (Ref. 19:140), "Whereas at overvoltages (high percent V_{SB} for the initial charge carriers, N_o, very large)* the space charge field is sufficient to start the streamer, in cooperation with the gas ionizing radiation, without a time delay ($\Delta t_d = 0$) *, the streamer start is also possible at lower overvoltages (smaller percent V_{SB} for N_o large)*, but needs a certain time delay $T_K (\Delta t_d)$ * to produce favorable conditions for this start. The physical process leading to the start of the streamer will be the same as that described above: gas ionizing radiation produces electrons around the positive ion cloud, which increases its carrier density; but here in the static breakdown case (low percent V_{SB} for N_o large)*, a large number of generations of such avalanches, started in the gas by the gas ionizing radiation, is necessary to

---

*Parenthesis inserted by the author.

accumulate step by step a sufficient charge density to start the streamer and to make the streamer visible as a steep current rise after a time T_K (Δt_d) *." ... "It may be that these avalanche generations run for a certain time with a nearly constant current just at the limit of being self-sustained; the value of this current can be small, so that it is not observed..." This statement, in conjunction with oscilloscope traces (Ref. 19:151-2), indicates that the current form should consist of an electron pulse followed by no measurable current, until at Δt_d a large current increase signals breakdown. The fast closure condition is necessary to correlate the observed laser-induced breakdown currents with the current traces by Raether.

The current form illustrated in Fig. 3 is typical of breakdown at about 60% V_{SB}. After certain time corrections it would be evident that the initial pulse--following the laser pulse and preceding breakdown--corresponds in time to a prompt current with a duration approximately the laser pulse duration and amplitude proportional to the laser pulse intensity. A change in the electric field from 3×10^4 volts/cm to 1.2×10^4 volts/cm did not appreciably change the duration of the current pulse. It is this behavior which

---

*Parenthesis inserted by the author.

leads one to suspect that a conducting path is formed by the laser, which closes shortly after the laser pulse terminates. To understand this we calculate the current due to a pulse of electrons traversing a gap.

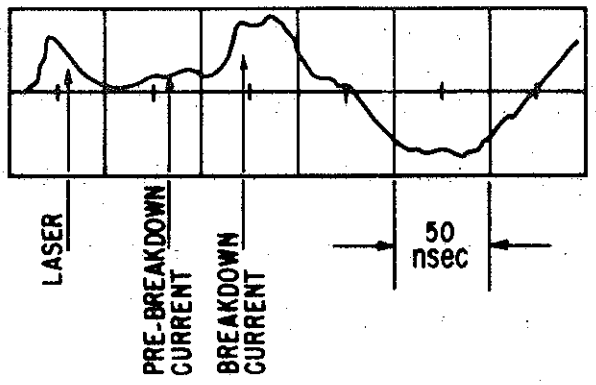

Fig. 3

OSCILLOSCOPE TRACE SHOWING LASER PULSE, PRE-BREAKDOWN CURRENT AND BREAKDOWN CURRENT.

Let N_o electrons simultaneously start from the cathode of a gap. If they move without multiplication in a field $E_o = U_o/d$ at a constant velocity v, an energy must be supplied of magnitude

$$\mathcal{E} = N_o e^{-E_o} \frac{dx}{dt} dt \tag{17}$$

or

$$\mathcal{E} = N_o e^{-E_o} V dt \tag{18}$$

since qE is the force experience by a charge q in a field E.

This energy must be supplied from an external charging circuit and is equal to

$$\mathcal{E} = UIdt \tag{19}$$

Then, $$UI = N_o \epsilon^- E_o V \tag{20}$$

or $$I = N_o \epsilon^- E_o V/(E_o d) \tag{21}$$

which simplifies to $$I = N_o \epsilon^- V/d \tag{22}$$

This current flows through the external charging circuit for the duration of the electron transit. At E/p = 35 volts/cm-torr, the electron transit time for the 11.6 mm gap used in this part of the study would be about 100 nsec, while the pre-breakdown current (Fig. 3) lasted for only 50-60 nsec. This indicates that electron transit cannot explain the current form. The fact that firing onto the anode produced identical results further supports the assertion that a highly conducting path is formed between the anode and cathode for the duration of the laser pulse. Temper this argument with the observation that at E/p = 20 volts/cm-torr, the transit time would increase to 140 nsec while the observed current remained constant in duration, and the validity of the assertion seems plausible.

It should be noted that the collapse of this conducting channel cannot be explained by the recombination of free

electrons with ions. The mean time for electron attachment in air at 760 torr and 20°C is given by Cobine (Ref. 4:97) as 630 nsec.

One explanation might be found in the rapid radial expansion of spark channels. If it can be argued that the laser-induced conducting path behaves as a highly stable spark channel, then it could be proposed that radial expansion of the conducting path lowers its carrier density (hence conductivity) and the current falls to zero. Radial expansion velocities to 10^6 cm/sec have been reported (Ref. 20:2). For a 0.4 mm diameter region of high conductivity, a time of 8 nsec is necessary for the conductivity to fall by half if the radial velocity is 10^6 cm/sec. Thus, nanosecond times of collapse may be accountable by radial expansion of the ionization path.

Laser Beam--Matter Interactions

Investigations of spark gap breakdown have usually been concerned with overvoltaged gaps. In this and similar studies of laser-induced breakdown, gaps charged below static breakdown voltage have been used. This is because the very large densities of charged particles produced by laser beams can trigger a gap without the aid of normal overvolting. Thus, it is appropriate to discuss some of the

observations and theoretical evaluations of the interaction of laser beams with matter.

It is generally agreed that for laser power densities of 10^5 to 10^8 watts/cm^2 at a metal surface, laser-induced electron emission is governed by the Richardson equation for thermionic emission (Ref. 3, 10, 13, 20, 21). A time delay between the impingement of the laser beam on the surface and the emission of charged particles has been explained on the basis of conventional heat transfer theory. The references quoted all dealt with targets which were mounted in vacuum, thus reducing emission of adsorbed gas to a minimum.

Higher power densities of 10^9 to 10^{10} watts/cm^2 have been used to study plasma production in metal surfaces and gases. Meyerand and Haught reported the electron density of a fully ionized plasma of 10^{19} cm^{-3} in the focal volume of a 40 MW laser focused in air (Ref. 16:8). The plasma appeared approximately five nsec after the arrival of the laser beam. It would be expected that higher power lasers could reduce the plasma formation time.

David, et.al., reported the production of an optically dense plasma at the surface of pyrolitic carbon (Ref. 5:493). Electron densities to 10^{19} cm^{-3} were reported from the interaction of the 160-400 MW beam with the carbon in vacuum. In a subsequent paper by Weichel and Avizonis,

plasma expansion velocities to 7 x 10^6 cm/sec, caused by thermal expansion of the plasma during absorption of the 40 MW laser pulse, were reported (Ref. 23:334). A time lapse of 60 nsec between the arrival of the laser pulse and the plasma formation was also reported. This study was conducted with a pyrolitic carbon target in vacuum.

An interesting study by Isenor (Ref. 11) reported a prompt emission of electrons which increased with increasing background gas pressure (10^{-5} to 10^{-3} torr). It was stated that the emission was enhanced by the adsorbed gas. This report of prompt emission for pressures above high vacuum ($\approx 10^{-8}$ torr) increases the author's confidence in the condition concerning the prompt emission of electrons and ions at atmospheric pressure.

The gas ionizing radiation observed in avalanches has its analog in the plasma formed by the impingement of a laser beam on a metal target. A. W. Ehler reported radiation centered about 210 Å emanating from a plasma produced at a tungsten target. The energy associated with such radiation is roughly 60 eV, while that associated with the 6943 Å laser beam is only 1.8 eV. Thus, the ionizing ability of the plasma radiation is much greater than the laser beam, particularly since multi-photon collisions are necessary for 1.8 eV photons to ionize gases with 7 eV ionization

potentials. Ehler also reported that the magnitude of the current collected from the anode was the same as that collected from the cathode. Dr. Ehler's postulated model is reproduced here as an argument for prompt plasma production. "Ordinarily a metal surface will reflect most of the visible radiation which strikes it. However, with the high power densities obtained with the focused laser pulse (of the order of 10^{10} watts cm^2), heating and evaporation of the metal surface will occur at the beginning of the laser pulse. The dense cloud of ejected atoms, ions, and electrons will be rapidly ionized and heated. The plasma electrons which absorb the incident laser radiation reach thermal equilibrium in times considerably less than 1 nsec, and the ions are heated in turn by the electrons in a time of about 1 nsec." This statement has been included to stress the rapidity of events which corroborates with findings in this study.

Finally, if a beam energy F (ergs/cm^2sec) is associated with a laser beam, an electric field can be ascribed to the beam from

$$F = c E^2/8\pi \qquad \text{(Ref. 8:295)} \qquad (23)$$

Values for fields calculated in this manner reach 10^8 to 10^9 volts/cm. This leads to the strong possibility of field

emission processes. A study of laser-induced field emission conducted by Peressini (Ref. 18) reported prompt electrons in a 0.3 torr atmosphere of an inert gas. A private communication from Dr. Peressini, however, assured the author that in the regions of interest (pressure and laser power) multiphoton ionization was much more probable (Ref. 9:60).

It should be noted that electron production not only takes place at the focus of a laser beam, but anywhere the power density is great enough. High brightness lasers, using long focal length lenses where fields have similar strengths for long lengths, have produced visible breakdown channels over lengths of several meters. The power density varied by a factor of 4 to 8 across the gap in the present study, thus, volume ionization of the dielectric cannot be dismissed.

It can be concluded from the preceding discussion that prompt plasma formation in gas adsorbing environments is to be expected for laser power densities greater than 10^8 watts/cm^2. Also, ionization and heating of the plasma so formed will occur for the duration of the laser pulse. Probably multi-photon ionization could explain the formation of a highly conducting path for the duration of the laser pulse. The prompt collapse of such a conducting path has not been reported elsewhere in the literature.

III. Equipment

Coaxial Triggering Apparatus

The laser-triggered switching apparatus (Fig. 4) consisted of a gas-filled spark gap, a power supply with which to charge the gap, and a ruby laser operated in giant pulse mode with which to initiate gap breakdown. In the previous study conducted by Pendleton and Guenther, the laser beam was aligned perpendicular to the inter-electrode dimension of a sphere-sphere gap. The beam was focused along the line joining the points of closest approach of the electrodes. It was found that the lowest delay times were achieved when the laser beam was focused on an electrode. Thus, one recommendation for further research was that a coaxial geometry should be used to improve switch response. The system employed in this study was a coaxial laser-triggering system, developed independently by Guenther and Barbini (Ref. 3). In coaxial triggering (Fig. 4) the laser is aligned along the inter-electrode dimension of the gap. A lens was mounted in a hollow electrode (shown in cross section in Fig. 4) through which the laser beam passed. The lens was adjustable so that the laser beam could be focused on the opposite switch electrode. In this manner the laser beam traveled along the most probable breakdown path. The

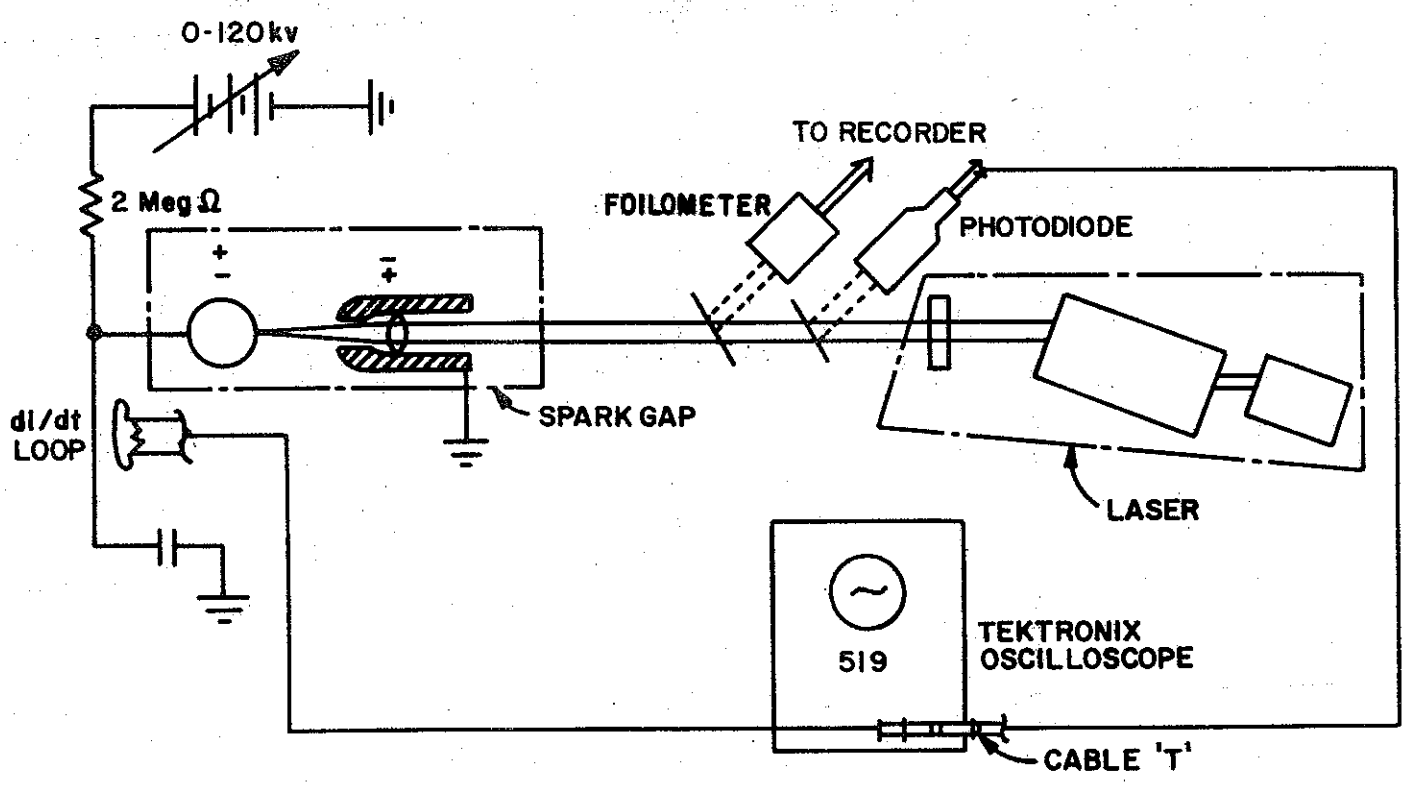

Fig. 4

SCHEMATIC DIAGRAM OF THE LASER-TRIGGERED SWITCHING APPARATUS

results of such an arrangement will be considered in a later section.

Spark Gaps

Three spark gaps were used in this investigation: a glass-walled atmospheric pressure vessel (620-640 torr in Albuquerque, New Mexico), a steel chamber which was used for pressures to 75 psia, and a unique coaxial capacitor which was charged by a Van de Graaff generator up to 1.5 megavolts.

The atmospheric pressure vessel consisted of a commercial, flanged, Kimax glass pipe with a pair of three-in. flanges and a pair of six-in. flanges. This spark gap was used for all the measurements in air at ambient pressure. Steel plates were affixed to the six-in.-diameter flanges on which the electrodes were mounted. A two-in.-diameter sphere was mounted on a 1/2-in.-threaded bolt which was fastened into one plate to form an adjustable electrode. A two-in.-diameter stainless steel hemisphere with a cylindrical base was threaded onto a two-in. O. D. stainless steel pipe which was threaded through the other plate. The interior of this electrode was drilled and tapped to accept a threaded lens mount. A conical section was removed from the hemispherical electrode through which the laser beam was focused on the spherical electrode. Gap spacing was

variable from zero to three cm. Electrical connections to the plates permitted charging the gap to 40 kV before corona losses became excessive.

A second spark gap was used which was designed to withstand pressure differentials of 20 atmospheres, although six atmospheres (75 psia) was never exceeded. It was constructed in the form of a 12-in. cube of welded 3/8-in. steel plate. Three, 2-in.-diameter viewing ports of 1/2-in. lucite were located on three sides, while the remaining side contained a six-in. access port. The electrode arrangement was the same as in the atmospheric cell, even to containing the same electrodes. The mounting bolt for the spherical electrode passed through a 1-1/2 in.-diameter nylon sleeve, which served to insulate the electrode from the grounded case. The hollow shaft of the remaining electrode screwed into the opposite face of the case and was flush with a three-in.-diameter, 1/2-in.-thick quartz window which was sealed to the case with an O-ring. Internal corona and breakdown along the dielectric insulating surface from the electrode mounting bolt to the case restricted the gap length to 1.5 cm. At the shorter gap spacing, breakdown occurred across the gap instead of between the bolt and the case. Potential differences of 100 kV were attained with this arrangement. The nylon sleeve used for mounting the

spherical electrode extended beyond the outside face of the cube. A lucite box was threaded onto the sleeve and was filled with transformer oil after the high voltage connections were made to the electrode mounting bolt, which extended through the sleeve, to prevent corona losses. The study of gap length-pressure effects in N_2 was made with this cell (to be described later).

The arrangements for charging and recording for both the cells just described were quite similar and will now be described. Two power supplies were used, both from Kilovolt Corporation. A 50 kV model was used to charge the atmospheric cell, and a 120 kV model was used for the high pressure cell. The cells were both charged through a two megohm charging resistor (Fig. 4), which was insulated with oil. The high voltage lead from the resistor was attached to a plate or to the mounting bolt, while the other electrode was returned to ground through a series of 30 kV-500 pf capacitors. Two 30 kV capacitors, in series, were used for the atmospheric cell (40 kV), and three, in series, were used for the pressure cell (90-100 kV). The low value of these capacitors was chosen to give the voltage pulse a fast rise time when the gap was discharged. The gap conduction was monitored by a single turn di/dt loop which was positioned near the cable which connected the capacitors to the electrode.

The third spark gap used in this study was a coaxial capacitor which was charged by a Van de Graaff generator (Fig. 5). It was designed with a characteristic impedance of 50 ohms and constructed by Ion Physics Corporation of Burlington, Massachusetts. It was designed for operation at a pressure of 400 psia and a maximum charging voltage of 1.5 megavolts. The Van de Graaff generator had a nine-in.-diameter column with a five-ft.-long by nine-in.-diameter terminal hung in cantilever suspension concentric with the 30-in.-diameter outer coaxial case. The terminal was capped with a hemispherical electrode which was opposed by a nine-in.-diameter hemispherical electrode across a gap which could be adjusted from zero to six in. A cylindrical 50 ohm $CuSO_4$ aqueous load was connected in series with the latter electrode to ground. A capacitive voltage divider was used to monitor the voltage pulse, and a resistive shunt was used to monitor the current. An optical path was provided through the aqueous load, and a lens internal to the grounded electrode focused the laser beam on the terminal electrode. The charging potential was monitored by a generating voltmeter that transforms a D.C. field into an A.C. signal with an amplitude proportional to the D.C. field.

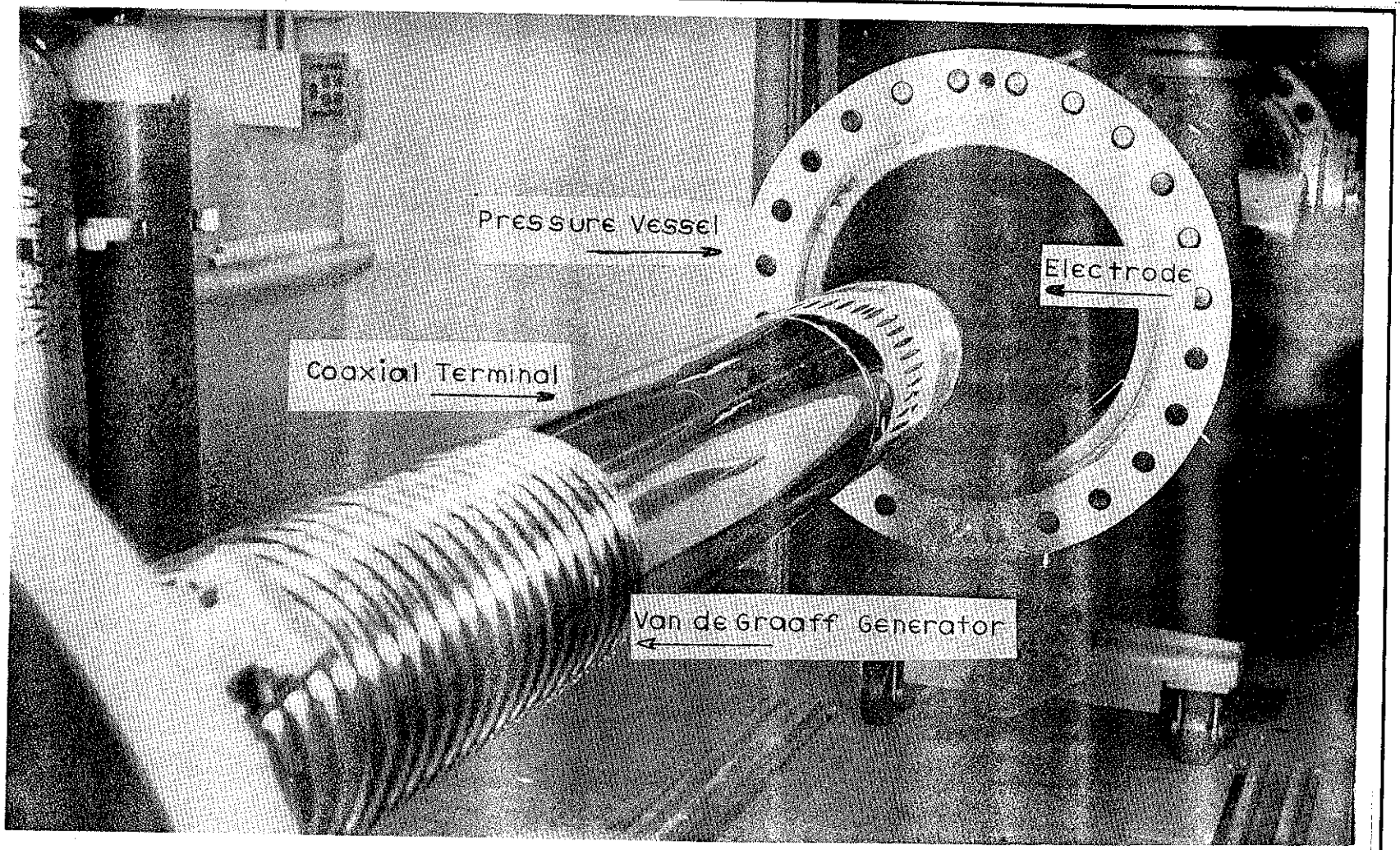

Fig. 5
MEGAVOLT TRIGGERING APPARATUS

Laser System

The laser used in this switching study was the Korad Corporation Model K-2Q ruby laser, operated in pulse mode. Energies from 1.4 to 6.2 joules, with pulse widths (FWHM) from 8.5 to 27 nsec, were obtained, depending on the Q-spoiling method used. Since the laser pulse was nearly gaussian, the average power was taken to be the quotient of the total energy in the beam and the pulse width at half intensity (FWHM). Power output, then, was from 80 MW to 300 MW. Brewster-angle cut ruby rods nine in. long by 3/4-in. in diameter were employed in the laser head. A single helical xenon flashlamp provided optical pumping. The majority of the data was taken at four-minute firing intervals. However, the acquisition of a 16-gallon, constant temperature laboratory bath ($\pm$ 0.06°C) permitted firing interval of two minutes, with a factor of six safety margin to prevent damage to the rod. The data obtained with the 1.5 megavolt generator was taken at two-minute firing intervals, as was the pre-breakdown current data. Two Q-spoilers were used: a passive, bleachable-dye cell and an active, Pockels Cell Q-spoiler.

Q-spoilers

The passive Q-spoiler consisted of a Brewster-entrance quartz prism, a hollow dye-cell, and a TIR (totally internal

reflecting) prism bonded together as one unit. The hollow cell is filled with a solution of cryptocyanine and methanol. The cryptocyanine absorbs the light from the ruby rod until enough energy has been absorbed to bleach the cryptocyanine. There follows a coherent burst of light from the laser, which constitutes the giant pulse. Optimization of the laser output consists of varying the concentration of the cryptocyanine until it bleaches through coincident in time with the maximum population inversion in the ruby rod. Because of its inherent simplicity (no mechanical or electrical components), it would seem ideal for a time limited research project. Offsetting the advantages of the cryptocyanine cell were three shortcomings: (1) Proper dye concentration was difficult to control. Since a change in only one part in 500 changed the operational mode from one of several pulses to no pulse at all, the dye concentration (coupled to the imput energy of the flashlamp) was quite critical. (2) Command jitter (i.e. variance in delay from laser firing command to actual laser firing) was $\pm$ 30 μsec. This meant that a switch with less than one nsec jitter was being triggered with an uncertainty of 30 μsec. (3) Unless dye concentration was perfect, low energy lasing preceded the giant pulse. It was found that when the gap was charged above 90% of its static breakdown voltage, the pre-lasing

could initiate gap breakdown before the giant pulse arrived. Since the low energy in the pre-lase was discriminated against in the oscilloscope triggering circuit, only the giant pulse was recorded, with the result that negative delay times were recorded. It was found that reproducible results could be obtained by slowly increasing the dye concentration until further addition of cryptocyanine failed to increase the delay between the laser pulse and the gap breakdown.

The Pockels Cell Q-spoiler used was an electro-optical active switch. Horizontally polarized light (the preferred plane of polarization of the ruby rods used) entered a horizontally oriented Brewster window. The light passed through the Pockels crystal unchanged in its major component of polarization and impinged on a stack of optical flats oriented at the Brewster angle for vertically polarized light. The horizontally polarized light was then scattered out of the optical cavity, thereby prohibiting lasing action. At a time set to coincide with optimum pumping energy, a 40 kV pulse was applied to the Pockels crystal, which retarded the light E vector, thereby rotating the plane of polarization by 90^{o}. This vertically polarized light fell on the Brewster stack and was transmitted to a TIR prism. The result was a coherent burst of light (the giant pulse)

which was rotated another 90° (back to horizontal polarization) on the passage through the Pockels crystal. The Pockels Cell had several advantages over the cryptocyanine cell: beam divergence was less (2-5 milliradians compared to 5-10 milliradians), command jitter was ± 7 nsec compared to ± 30 μsec, it readily produced a single pulse with good reproducibility, and it prohibited pre-lasing and post-lasing.

Auxiliary Equipment

Several pieces of equipment were used for diagnostic purposes, and a brief description of each follows.

For the two small gaps, charging voltages were measured with electrostatic voltmeters. Sensitive Research Instruments Model ESH, with a 100 kV maximum deflection, was used with the pressure cell, and Sensitive Research Instruments Model ESH, with 10, 25, and 50 kV scales, was used in conjunction with the atmospheric cell. Calibrations furnished gave accuracy to 1%.

An ITT Biplanar S-20 photodiode, capable of a 0.68 nsec risetime and less than 1.0 nsec delay, was used to monitor a portion of the laser beam for pulse shapes and timing purposes.

A Tektronix type 519 oscilloscope was used to record the photodiode traces and breakdown voltage data. A Polaroid

scope camera was used with type 410 film (ASA 10,000) to record the oscilloscope traces. A sine wave generator, which gave output frequencies up to 500 Mc, was used to calibrate the horizontal sweep rate. The frequency of the sine wave was monitored by a digital frequency monitor with accuracy to one cycle in 10^9 quoted in its manual. Photographs were taken of the sine waves at each sweep speed for varying sinusoidal frequencies. The oscilloscopes were then calibrated at each millimeter of horizontal sweep, and the calibrations were reproduced graphically (Fig. 6). In this manner, times to one nanosecond were easily readable at 20 nsec/cm sweeps. Such a calibration procedure had to be followed, since the first millimeter of horizontal sweep is non-linear on type 519 oscilloscopes.

The oscilloscope trace photographs were read on a Carl Zeiss Model 1047 film reader. This device, with typewriter readout, had a reproducibility of ± 1.0 micron. This accuracy, however, was severely limited by operator error to ± 0.08 mm when reading laser starting points and ± 0.07 mm when reading breakdown starting points (see Appendix A for translation of these distance inaccuracies into time inaccuracies).

Laser energy was monitored by a thin foil calorimeter (foilometer). (C. W. Bruce and E. Collet, "Laser

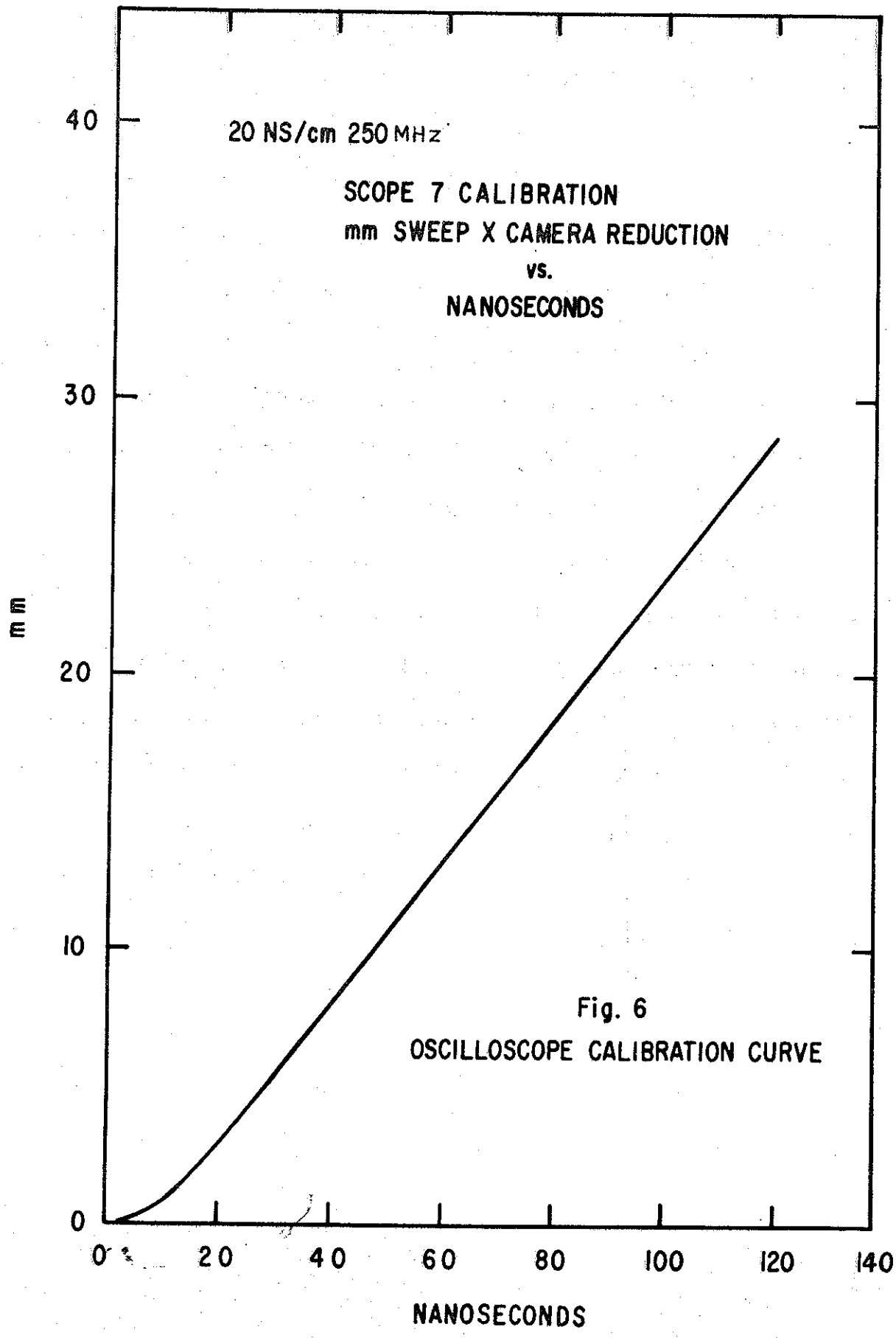

Fig. 6
OSCILLOSCOPE CALIBRATION CURVE

Instrumentation," Kirtland AFB, New Mexico. AFWL TR-64-127, AD364551, June 1965) A portion of the beam was reflected onto a square piece of aluminum foil which had a thermocouple on its back side. The foil was calibrated against a hollow silver sphere calorimeter of known mass (Ref. 23:335).

The output of the foilometer was displayed on a Sanborn Model 7700 heated stylus-strip chart recorder. Typical sensitivities were about 0.1 joules/mm, and the foilometer displaced the stylus an average of 20 mm.

Electrical lengths of coaxial cables were measured with a Hewlett-Packard Time Domain Reflectometer. All of the cables were measured at the 20 nsec/cm sweep rate setting. The distance measurements on the viewing grid were accurate to 0.01 cm, for an error of 0.2 nsec in total sweep, or only 0.1 nsec for total length. This is true since the actual length was half the electrical length from the output pulse to the reversed pulse.

IV. Experimental Techniques

System Parameters

The influence of the following parameters on switch performance were studied: the percentage of the self breakdown voltage to which the gap was charged ($\%V_{SB} = V_{CH}/V_{SB} \times 100$, where V_{CH} = charging voltage), dielectric medium and pressure (p), laser energy and pulse shape, polarity of the gap (including the grounding arrangement), the reduced field in the gap (E/p), and the material used for the target electrode. The parameters were determined in the following manners. Self breakdown voltage was found by slowly increasing the charging voltage until gap breakdown occurred. Five such determinations were taken as an adequate measure of V_{SB}. The ratio of the electrode diameter to gap spacing was always greater than 4:1. This constitutes a well defined gap, according to Meek and Craggs (Ref. 15:312), in which breakdown characteristics will follow Paschen's Law. That is, V_{SB} is linearly dependent on pd in the ranges used in the experiments, thus unless pd varied V_{SB} determinations were made only twice daily.* Owing to corona effects and

*It should be noted that daily variation in relative humidity were slight in Albuquerque and was between 30 and 40%.

field enhancement due to non-uniform electrodes, V_{SB} was determined for each polarity.

Gap spacing was taken to be the distance of closest approach of the electrodes. Since one electrode had a coaxial opening to pass the laser beam, inside calipers could not be used. Instead, calibrated thickness blocks were used for measuring gap spacing (Fig. 7).

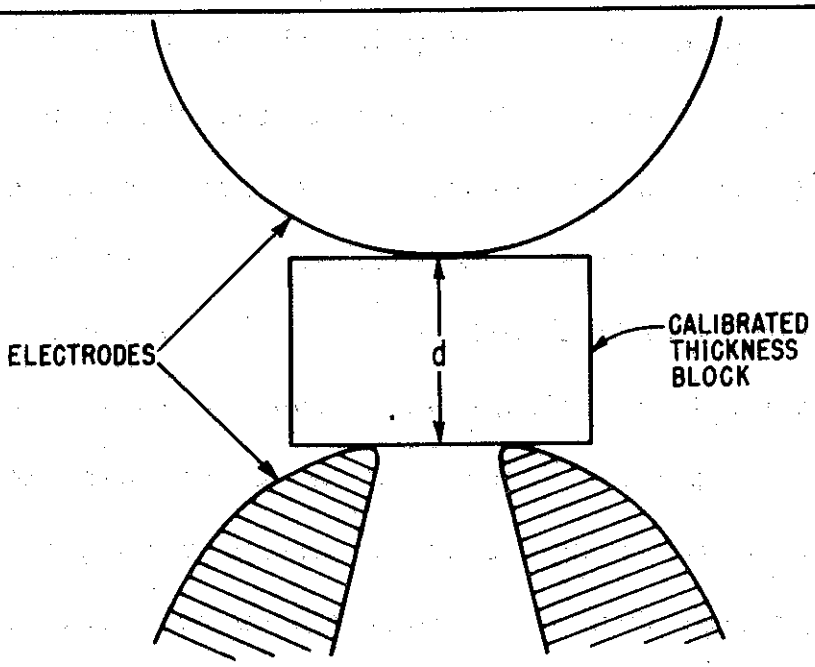

Fig. 7

METHOD FOR DETERMINING THE GAP SPACING

Charging voltage was measured with the electrostatic voltmeters on the small gaps and with the generating voltmeter on the large gap. The generating voltmeter had to be calibrated since it was not an absolute device. The terminal of the Van de Graaff generator was connected to ground

through a series of twenty 10-gigohm resistors. A microammeter monitored the leakage current in these resistors. A conversion could then be made between charging voltage, V_{CH}, and leakage current, i_1, in this manner:

$$V_{CH} = i_1(20 \times 10 \times 10^9) \text{volts} \tag{24}$$

for i_1 in amps, or

$$V_{CH} = 0.2 \cdot i_1 \text{ MV} \tag{25}$$

for i_1 in microamps. This method cannot be used for any extended period, however, since the resistors degrade with voltage, temperature, and time. Thus, the secondary standard (the generating voltmeter) was used.

The dielectric medium in the gap was recorded on each shot, as was the pressure of the gas dielectrics. Atmospheric pressure was monitored with an aneroid barometer which had a limit of accuracy of $\pm$ 0.1 torr. In the pressure gaps atmospheric pressure and gauge pressure were both monitored to give absolute pressure to $\pm$ 50 torr.

Laser energy and laser pulse shape were monitored as described in the preceding section.

Electrode polarity was recorded in such a way that there were four polarity arrangements--these are: (1) Cathode as target electrode/cathode grounded, (2) Cathode as target

electrode/anode grounded, (3) Anode as target electrode/anode grounded, and (4) Anode as target electrode/cathode grounded.

Diagnostic System

Figure 8 is a schematic of the diagnostic system. Cable lengths were measured as described in section III. Time of flight delays were measured with a steel tape. Since the velocity of electromagnetic waves is C = 29.998 cm/nsec (in vacuum), an error of ± 1 cm meant an inaccuracy of only about ± 0.03 nsec, which was an order of magnitude below other errors. In dielectric or conducting media, the speed of electromagnetic radiation is $c/\sqrt{\mu\epsilon}$, where μ is the permiability and ϵ is the dielectric constant (Ref. 12: 203). This correction had to be made for cables which could not be checked on the Reflectometer and for other electrical connections.

The 519 oscilloscope was triggered internally by the photodiode pulse which was subsequently displayed. Cable lengths and sweep rates were chosen so that both the laser pulse and breakdown pulse were displayed on the same trace. Both the photodiode and di/dt cables were fed into the signal input of the 519, via a coaxial cable T. Insertion units with calibrated resistances were used to provide impedance matching and thus reduce reflections. It was also

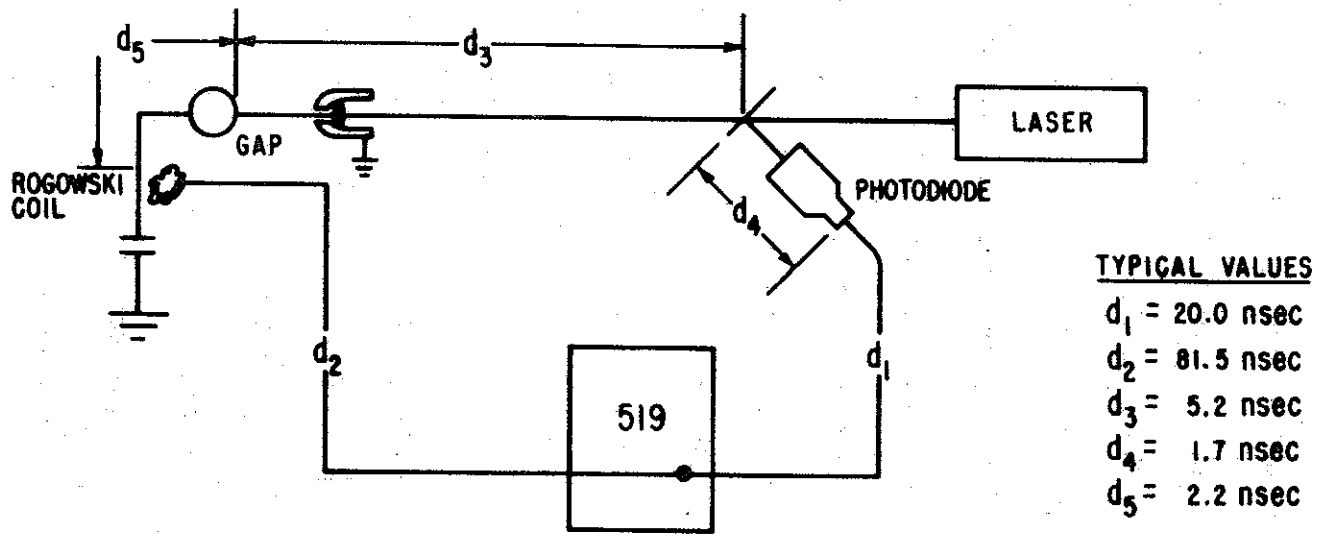

TYPICAL VALUES

d_1 = 20.0 nsec
d_2 = 81.5 nsec
d_3 = 5.2 nsec
d_4 = 1.7 nsec
d_5 = 2.2 nsec

Fig. 8

CABLE DELAYS AND TIME OF FLIGHT DELAYS IN THE SYSTEM

important to properly terminate each cable at the T or reflections would occur. For this purpose the 50-125 ohm adapters were chosen, such that the incoming cable was fed into the non-terminated end of the connector, while the cable T was fed with the terminated end of the connector. To adapt from a 50 ohm cable to a 125 ohm cable T with an in-line attenuator, it was only necessary to adapt the 50 ohm cable to a 125 ohm attenuator through a doubly non-terminated 50-125 ohm adapter. The reason for this is that all the attenuators are properly terminated to reduce reflections. Signal delay was found by determining the time for the start of breakdown from the beginning of the sweep and subtracting the time for the laser start from the beginning of the sweep. Triggering delay was then found by subtracting the cable length distances and the time of flight of the laser pulse from the signal delay. Figure 9 illustrates the procedure used to determine the signal time. The straightest portion of the signal rise was extrapolated to the base line, and this point was arbitrarily taken as the signal time. The signal delay was then determined by subtracting the time for point A from the time for point B.

Since there is a current which flows in the gap during the laser pulse, regardless of whether or not breakdown occurs during this period, a method was necessary to separate

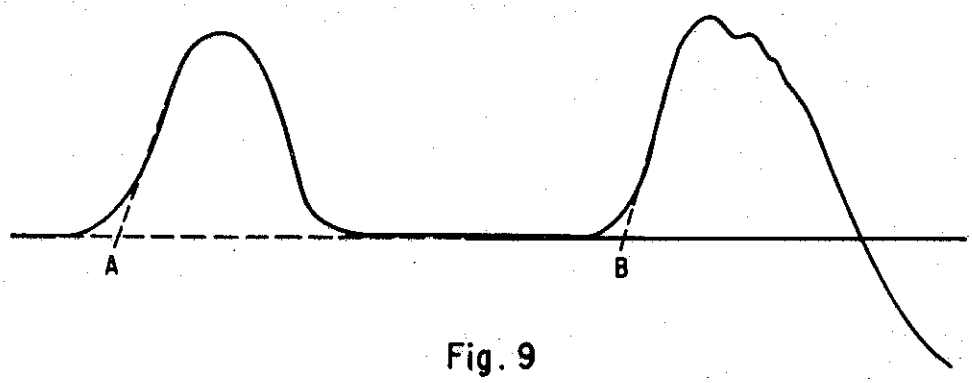

Fig. 9

METHOD USED TO DETERMINE SIGNAL TIMES

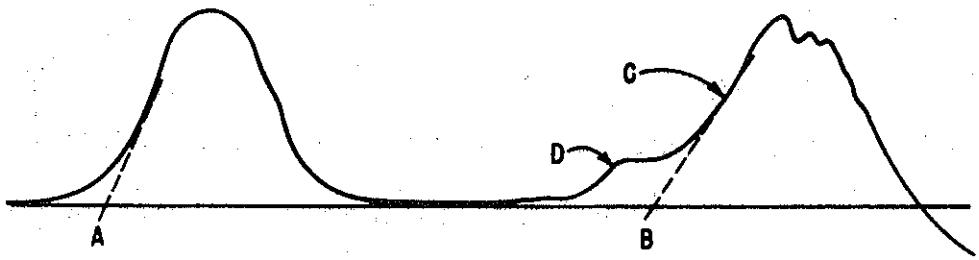

Fig. 10

METHOD USED TO SEPARATE BREAKDOWN CURRENT (C)
FROM PRE-BREAKDOWN CURRENT (D)

the pre-breakdown current from the breakdown current. Figure 10 illustrates a typical determination of this type. For laser powers in the 80 to 200 MW range the pre-breakdown current was less than a third of the breakdown current, and the separation posed no problem once its presence was categorized.

Special Procedures for the FX-15

Some special procedures were needed for the FX-15 megavolt supply. Since a dew point of less than -60°C was needed to operate the machine, dryness of the interior was requisite. Each time the pressure seal was broken it was necessary to wipe the interior with moisture absorbing cloths. Before the tank was pressurized it was evacuated to ≈10 microns Hg to reduce water and air content in the chamber. Careful measurement of the vacuum was not attempted, but relying on the manufacturer's claim for the roughing pump, a roughing period of six to eight hours was assumed to be adequate. The tank was then filled with laboratory gas with dew points between -60°C and -80°C.

V. Discussion of Data

Raw Data

The data which was used to determine the delay times Δt_d consisted of polaroid photographs of oscilloscope traces. The system parameters were measured as described in sections III and IV and were recorded in tabular form. Each oscilloscope trace was numbered and the same number was used to refer to all data taken on the particular shot. In addition to the oscilloscope traces and parameter monitors, time integrated photographs of the breakdown spark revealed pertinent information concerning the breakdown process. The following traces and photographs are typical of all the data collected during this study.

Figure 11 is a trace which shows the laser pulse followed by breakdown. The oscillation in the breakdown current is a result of the discharging characteristics of the capacitive circuit (Fig. 4). The following information pertains to this trace: V_{SB} = 35.2 kV, V_{CH} = 23.0 kV, target electrode = tungsten cathode, grounded electrode = cathode, sweep rate = 50 nsec/cm, Δt_d = 69.2 nsec, and laser power = 85 MW.

Figure 12 is a trace which shows the laser pulse followed by a pre-breakdown current which is followed by

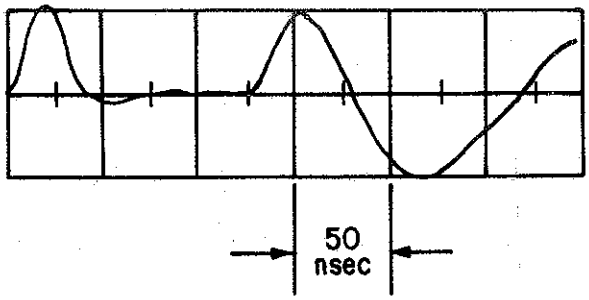

23.0 kv/35.2 kv = % V_{SB}
Δt_d = 69.2 nsec
LASER POWER = 85MW

Fig. 11

BREAKDOWN WITHOUT PRE-BREAKDOWN CURRENT

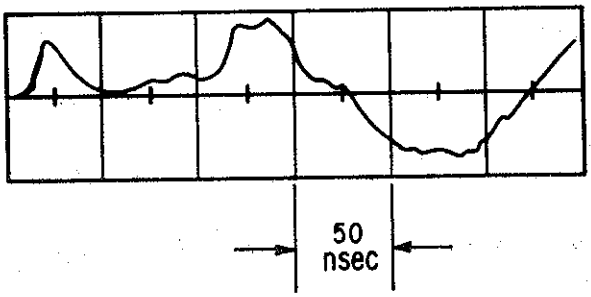

23.0 kv/35.2 kv = % V_{SB}
Δt_d = 34.7 nsec
LASER POWER = 150 MW (X2 ATTENUATION)

Fig. 12

BREAKDOWN WITH PRE-BREAKDOWN CURRENT

breakdown. Traces such as Fig. 12 led to the study of the pre-breakdown current as a function of the laser power and the field in the gap. Here laser power is 150 MW.

Figures 13 and 14 are arc photographs and the corresponding oscilloscope traces for a charging voltage of 600 kV. It was found that at certain laser power densities the jitter was inexplicably large. Figure 13 shows a breakdown with many lossy leaders. The corresponding oscilloscope trace at a sweep rate of 20 nsec/cm fails to record the breakdown. Figure 14 exhibits breakdown which is physically a highly linear saprk, therefore nearly lossless and exceedingly fast. The pulse which follows the laser pulse on the oscilloscope trace is the voltage pulse. The pulse duration is 10 nsec because the inner conductor of the system was five feet long, which gives a reflected pulse about 10 nsec in duration.

After reading the oscilloscope traces and making the delay corrections, the final data was reduced to graphical form.

Final Data

Figures 15 through 30 are graphs which are representative of the results obtained during this study.

Fig. 15. This is a plot of the delay time, Δt_d, vs. $\%V_{SB}$. Since pressure was nearly constant (atmospheric

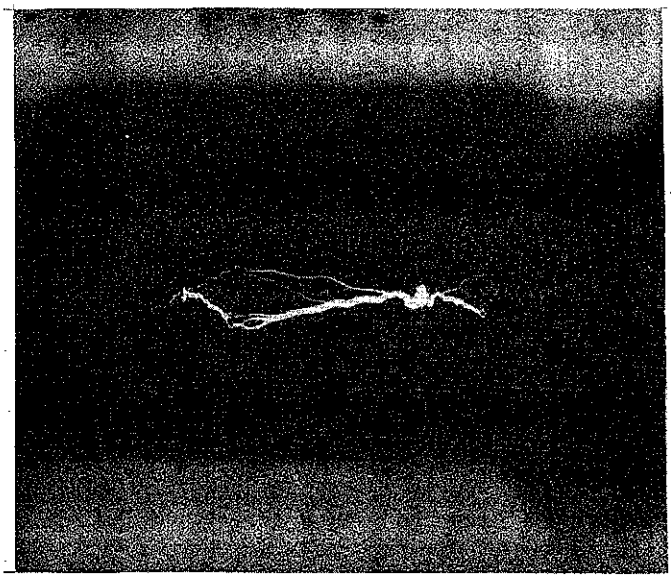

DIRECTION OF LASER BEAM ⟶

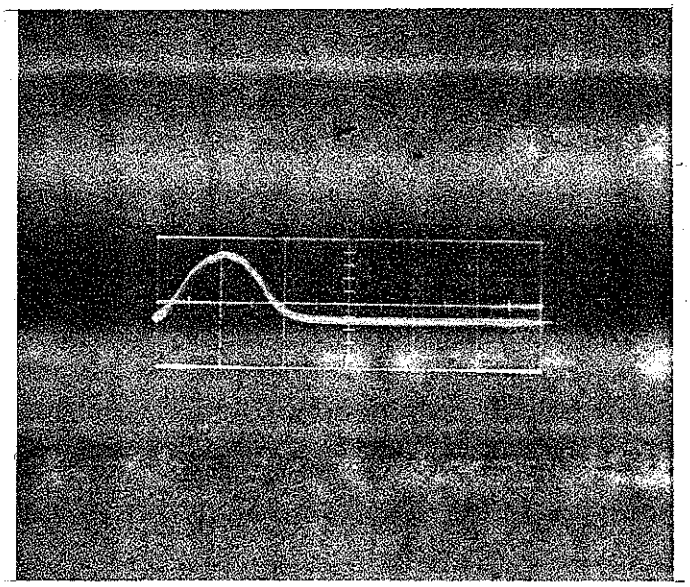

Fig.13

BREAKDOWN WITH LOSSY LEADERS

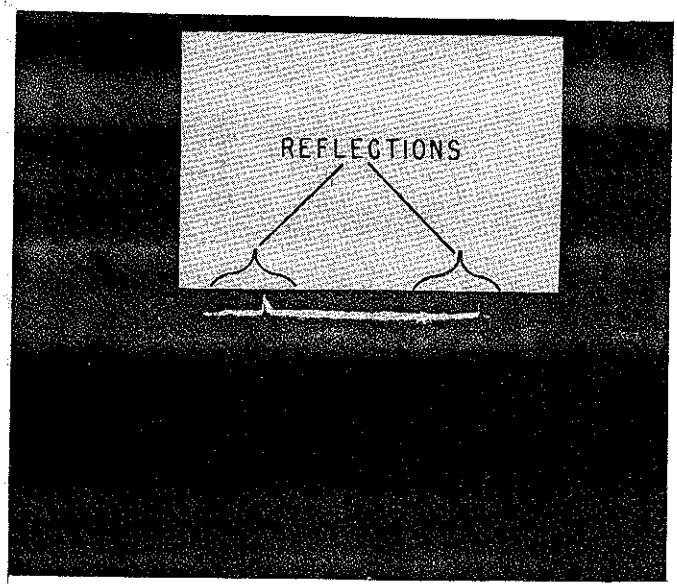

DIRECTION OF LASER BEAM ⟶

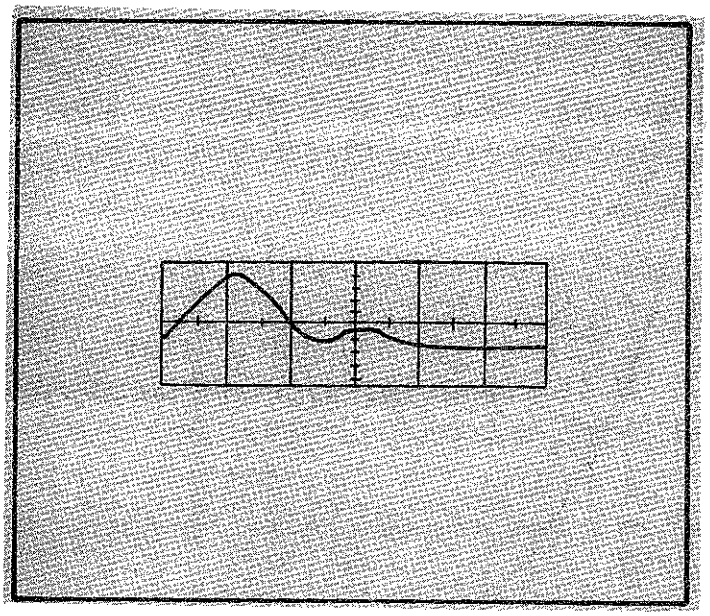

Fig. 14

STRAIGHT-CHANNEL BREAKDOWN

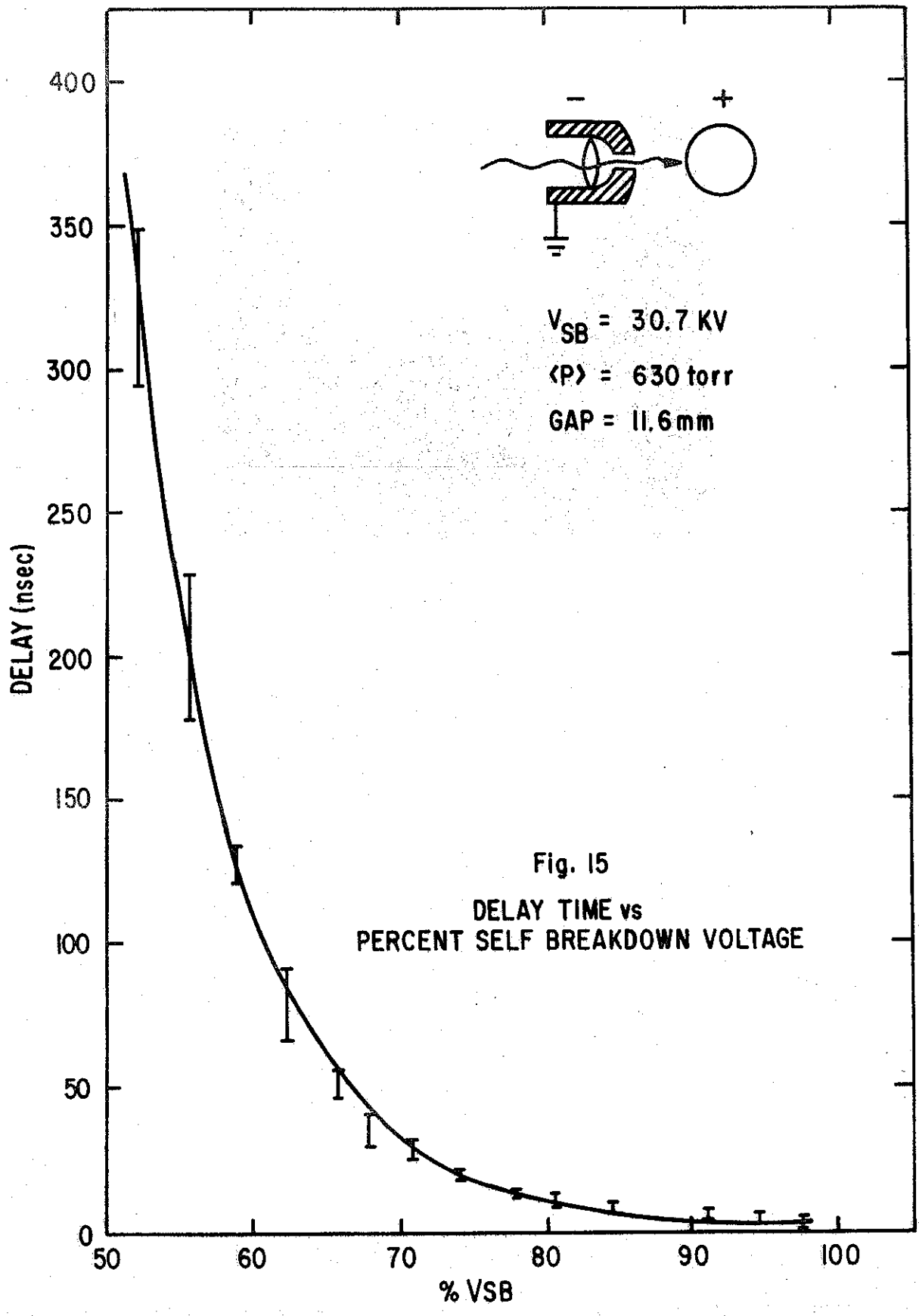

Fig. 15

DELAY TIME vs
PERCENT SELF BREAKDOWN VOLTAGE

pressure) during the period this data was obtained, Fig. 15 also indicates the strong dependence of delay time on reduced field (E/p). The error bars are an indication of the switch jitter. The laser power was kept between 130 MW and 165 MW. The indicated polarity is anode target/cathode grounded.

The scatter of the data points in the horizontal direction in Figs. 16, 17, 18, and 19 is not as great as first appearances would suggest. The horizontal scale has been expanded by a factor of six for increased readability.

Fig. 16. This is a logarithmic plot of delay vs. reduced field. This graph contains the same information as Fig. 15. The advantage of plotting Δt_d vs. E/p on a full logarithmic graph is that the dependence of Δt_d on E/p can more readily be determined by finding the slope of the straight line. In this instance the equation would be

$$\Delta t_d = A_1 (E/p)^{-8.27} \tag{26}$$

Fig. 17. This graph represents data taken with the cathode as the target and the anode grounded. This data was taken at the same time as that represented in Figs. 15 and 16. Since the power supply used in this part of the experiment could be readily switched from positive to negative output, a prescribed number of shots were taken at each

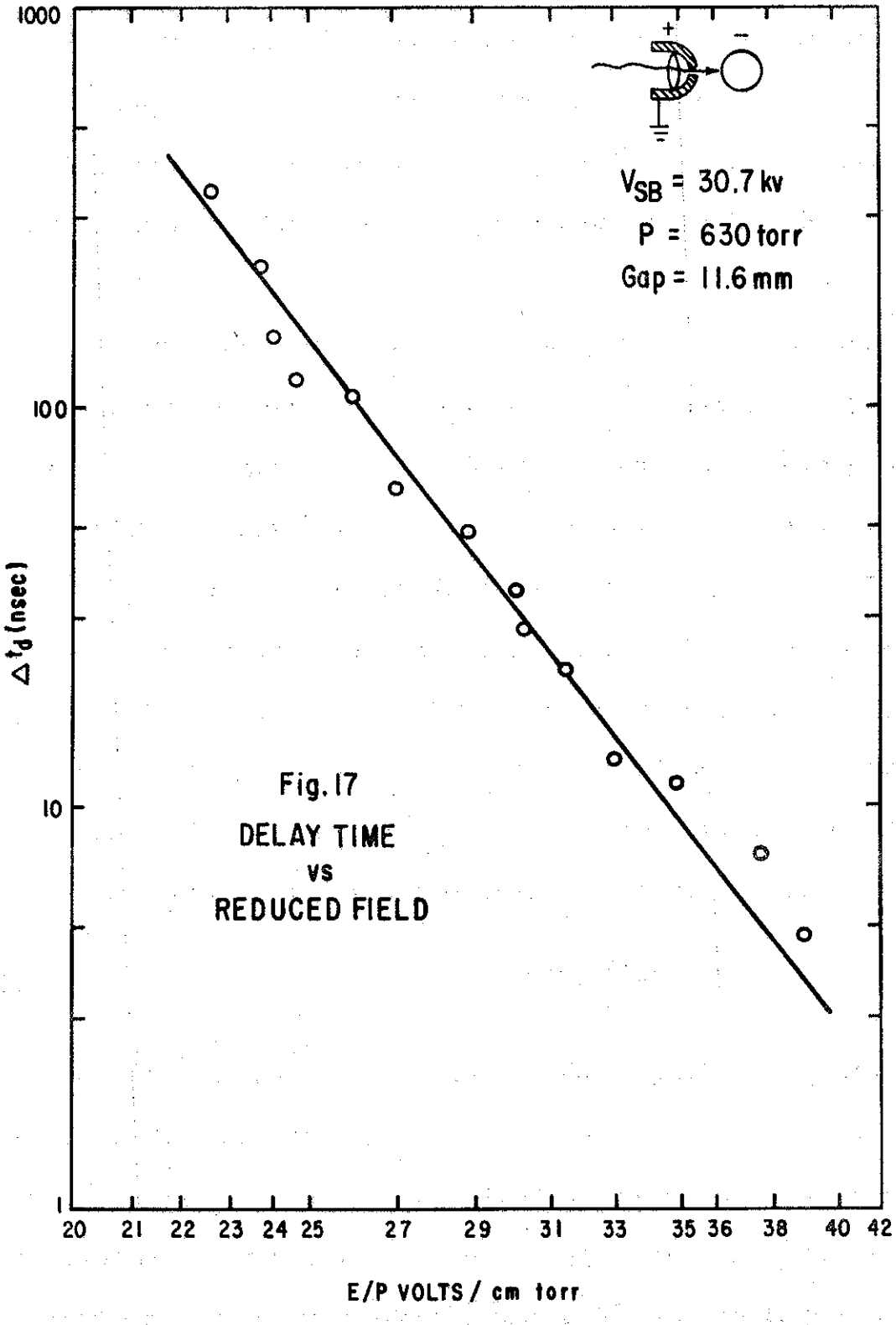

Fig. 17
DELAY TIME
vs
REDUCED FIELD

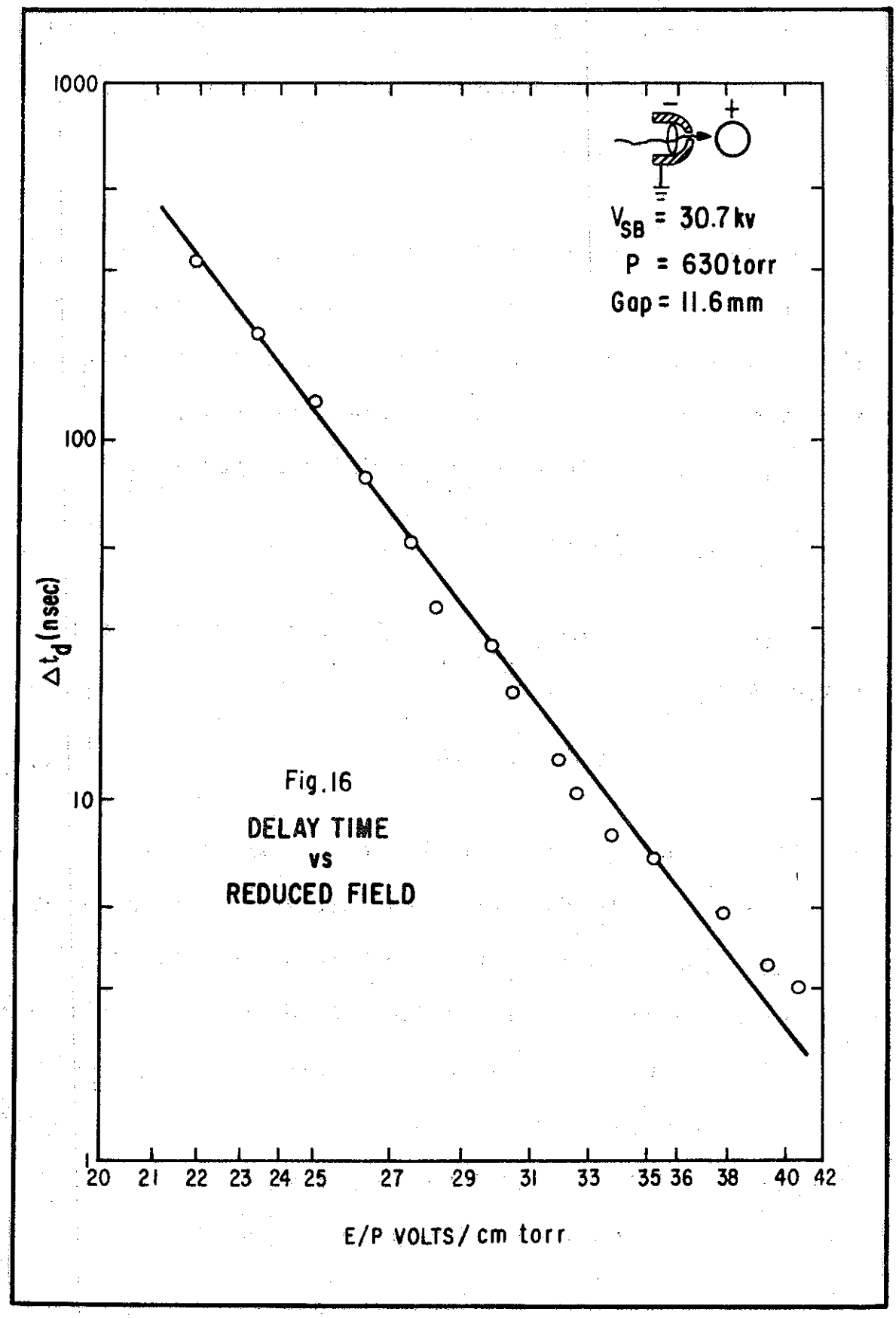
1000
100
10
1
Δt_d (nsec)
20 21 22 23 24 25 27 29 31 33 35 36 38 40 42
E/P VOLTS / cm torr
V_{SB} = 30.7 kv
P = 630 torr
Gap = 11.6 mm
Fig. 16
DELAY TIME
vs
REDUCED FIELD

voltage with both positive and negative targets. The empirical formula which gives the best fit to the data is

$$\Delta t_d = A_2 (E/p)^{-8.47} \tag{27}$$

The dielectric was air at ambient pressure.

Fig. 18. This graph and the one in Fig. 19 reproduce the results in Figs. 16 and 17, with the exception that the target electrode is also the grounded electrode.

From Fig. 18 the grounded anode as target gives

$$\Delta t_d = A_3 (E/p)^{-10.6} \tag{28}$$

Fig. 19. The empirical fit for the grounded cathode as target arrangement becomes

$$\Delta t_d = A_4 (E/p)^{-11.6} \tag{29}$$

It will also be noticed that the scatter increased from Fig. 16 to Fig. 19. The dielectric was air at ambient pressure.

Fig. 20. This is a superposition of two graphs. Plotted on the basic graph is electron drift velocity in air vs. reduced field. Superimposed on this is $d/\Delta t_d$ vs E/p. The function $d/\Delta t_d$ represents a "velocity" for the breakdown process. In Fig. 20 it can be seen that the delay time is not strongly dependent on electron drift velocity.

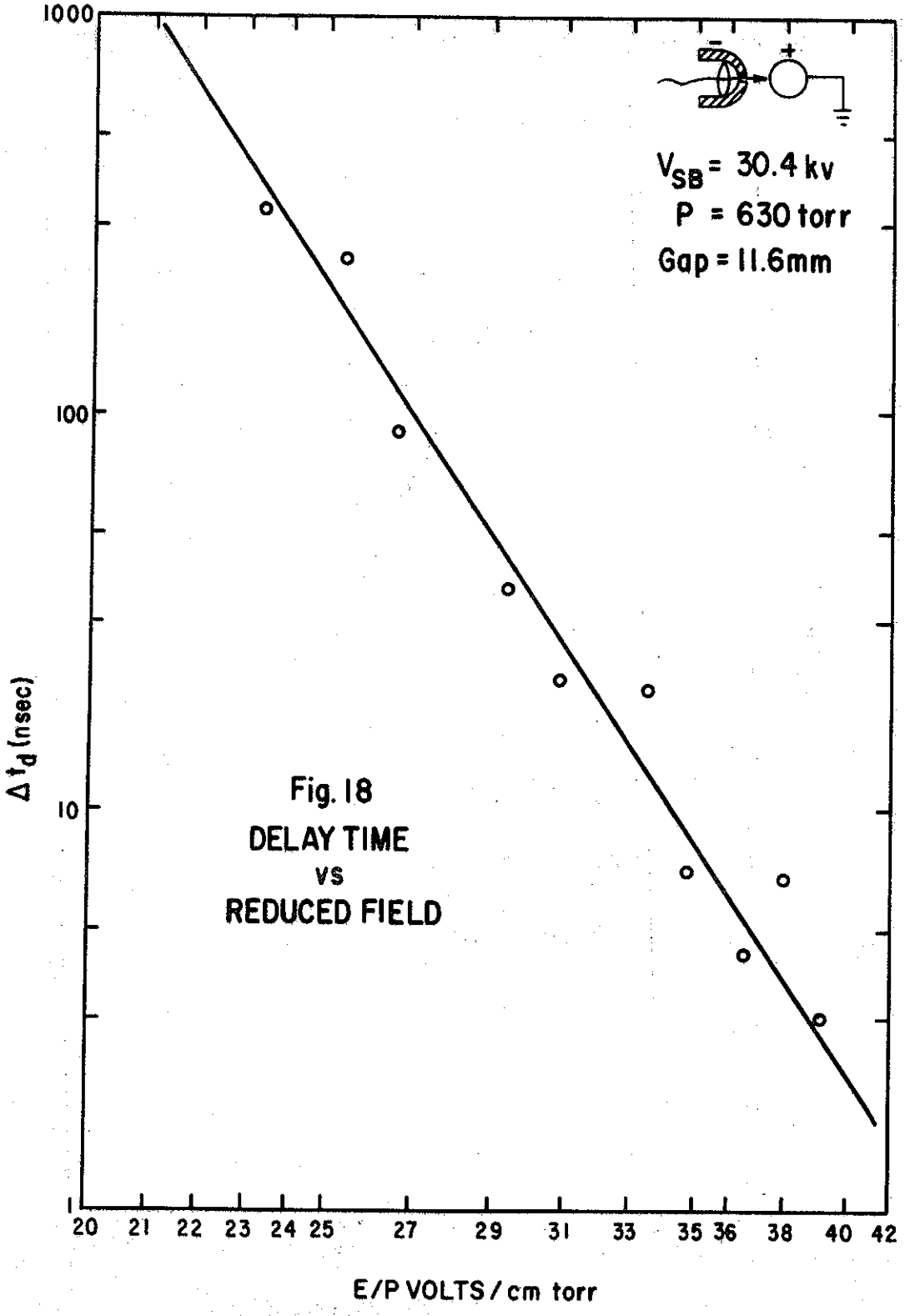

Fig. 18
DELAY TIME
vs
REDUCED FIELD

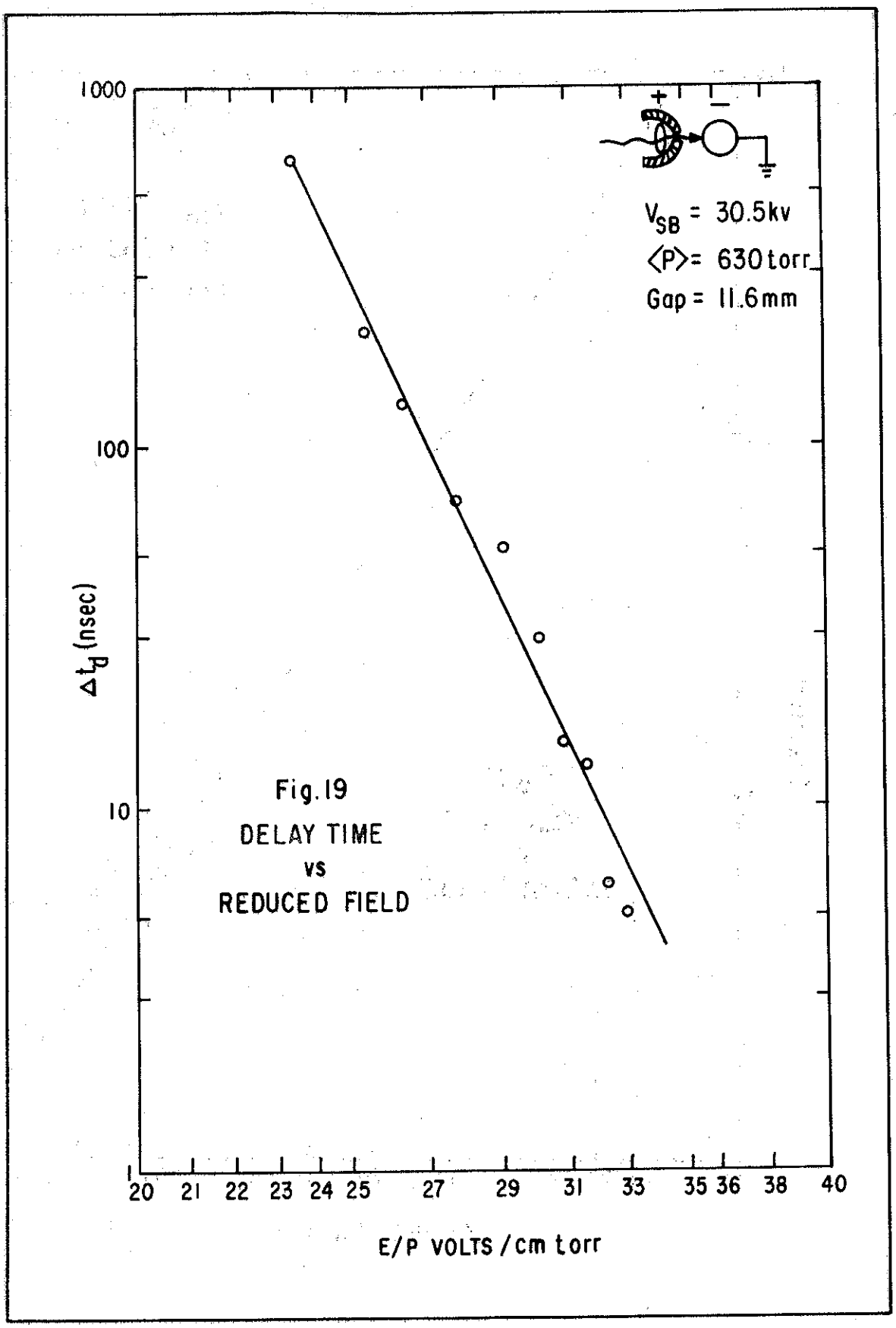

Fig. 19
DELAY TIME
vs
REDUCED FIELD

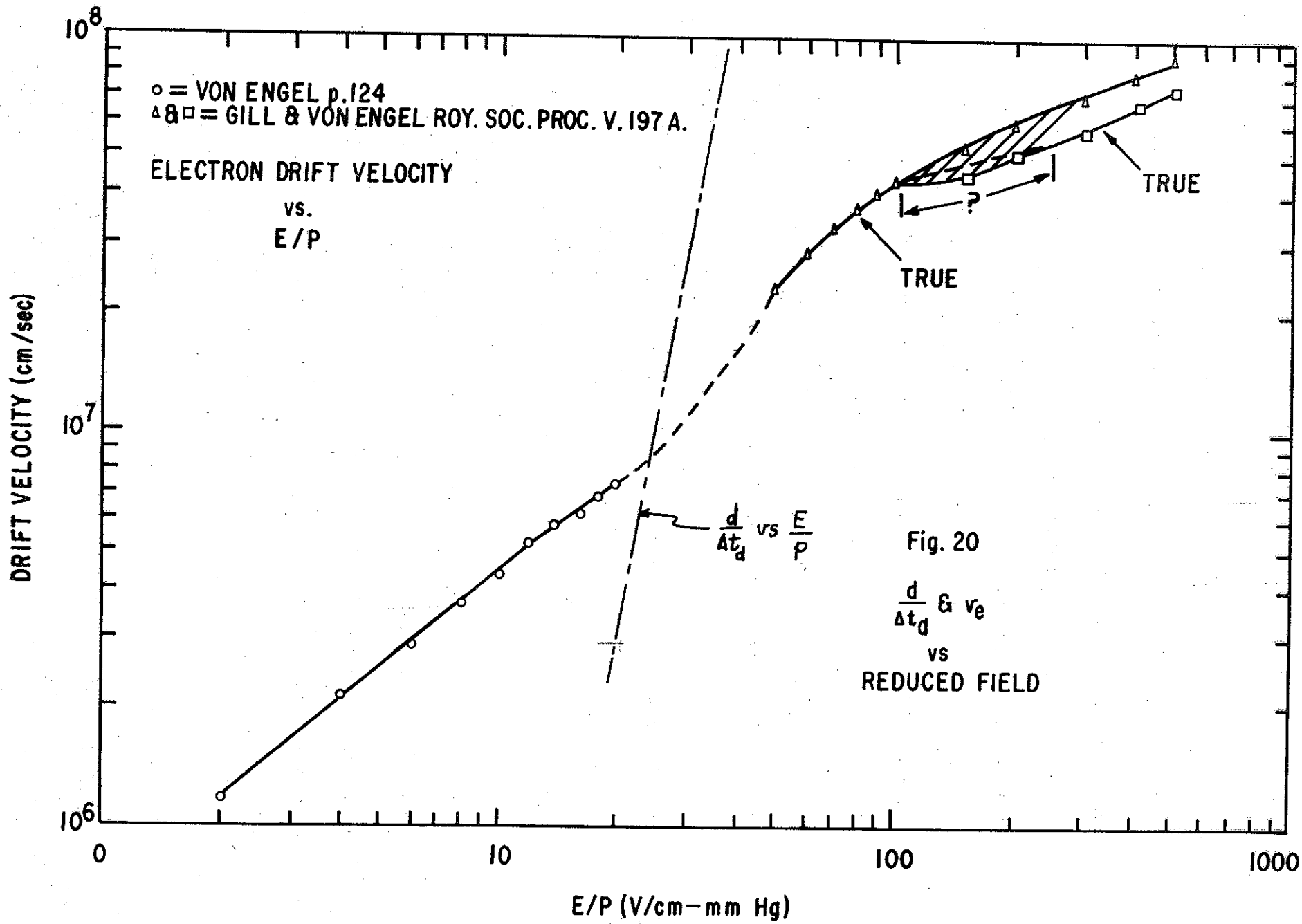

Fig. 20

$\frac{d}{\Delta t_d}$ & v_e
vs
REDUCED FIELD

Fig. 21. The switch jitter for the four polarities was quite similar, therefore only one is reproduced here. The general form of the dependence of jitter on $\%V_{SB}$ was the same--the only difference being the slope of the rapidly increasing portion. The nearly flat portion of the jitter vs. $\%V_{SB}$ extends down to the point where the delay (Fig. 15) is about 30-40 nsec. This delay corresponds to a rapid decrease in the laser intensity in the gap (Fig. 11).

Fig. 22. This bar graph shows the distribution of a set of 11 shots which were taken to determine the switch jitter. This data was taken at 97.5% V_{SB} when V_{SB} = 30.7 kV. The delay was 3.2 nsec with a jitter of $\pm$ 0.99 nsec.

Fig. 23. The work done in N_2 with pressures up to 3780 torr is represented in Figs. 23 and 24. Although it was previously determined by Pendleton that at a constant reduced field the delay time decreased with increasing pressure, the data in Fig. 23 was taken to confirm this dependence for coaxial triggering. In Fig. 23 the upper curve is for d = 7.5 mm, p = 2375 torr, and V_{SB} = 61.0 kV. The lower curve plots the data obtained with d = 7.5 mm, p = 3780 torr, and V_{SB} = 87.2 kV. The reduced field at V_{SB} was 34.3 volts/cm-torr for p = 2375 torr, and the reduced field at V_{SB} was 30.8 volts/cm-torr for p = 3780 torr.

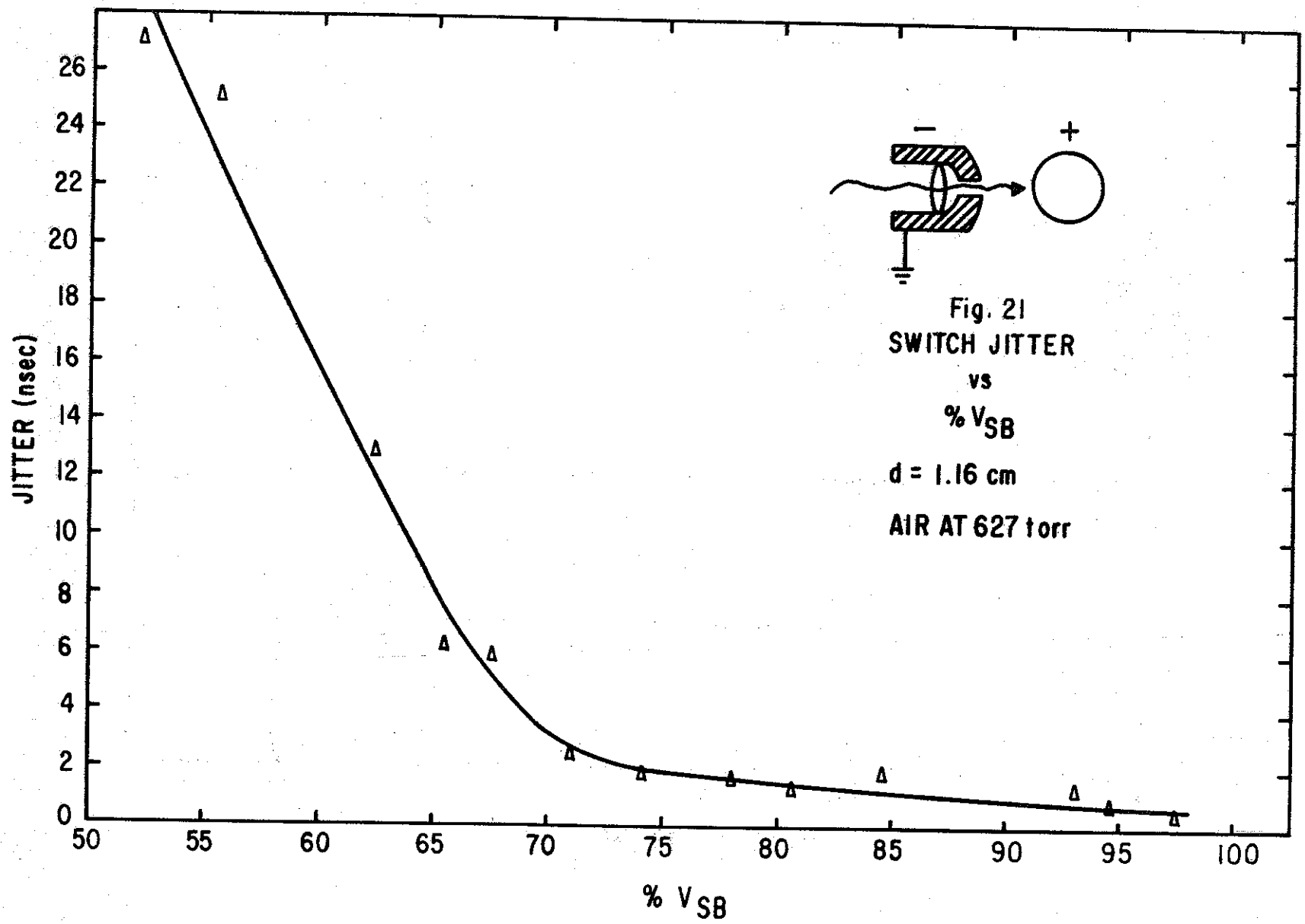

Fig. 21
SWITCH JITTER
vs
% V_{SB}
d = 1.16 cm
AIR AT 627 torr

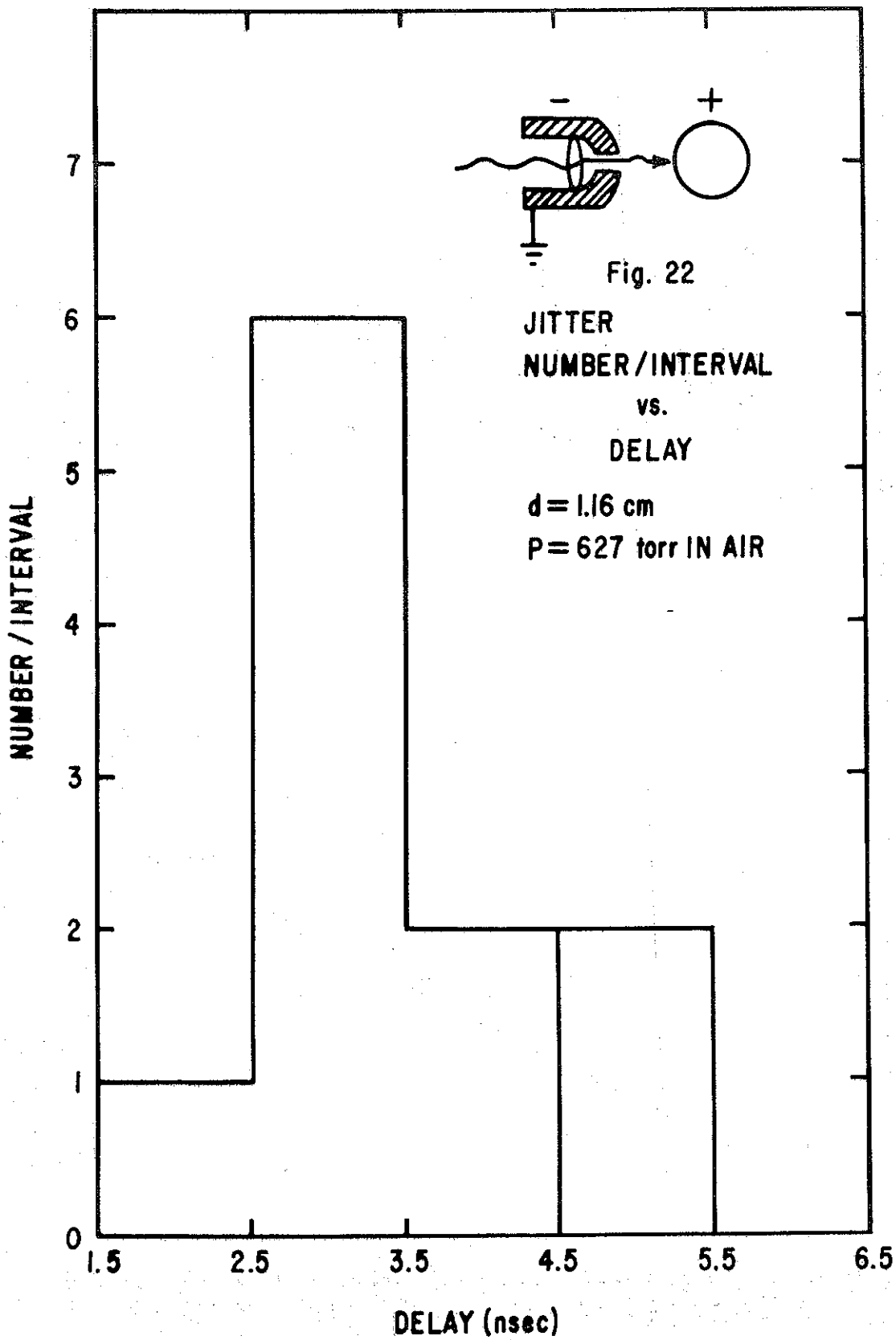

Fig. 22

JITTER
NUMBER / INTERVAL
vs.
DELAY

d = 1.16 cm
P = 627 torr IN AIR

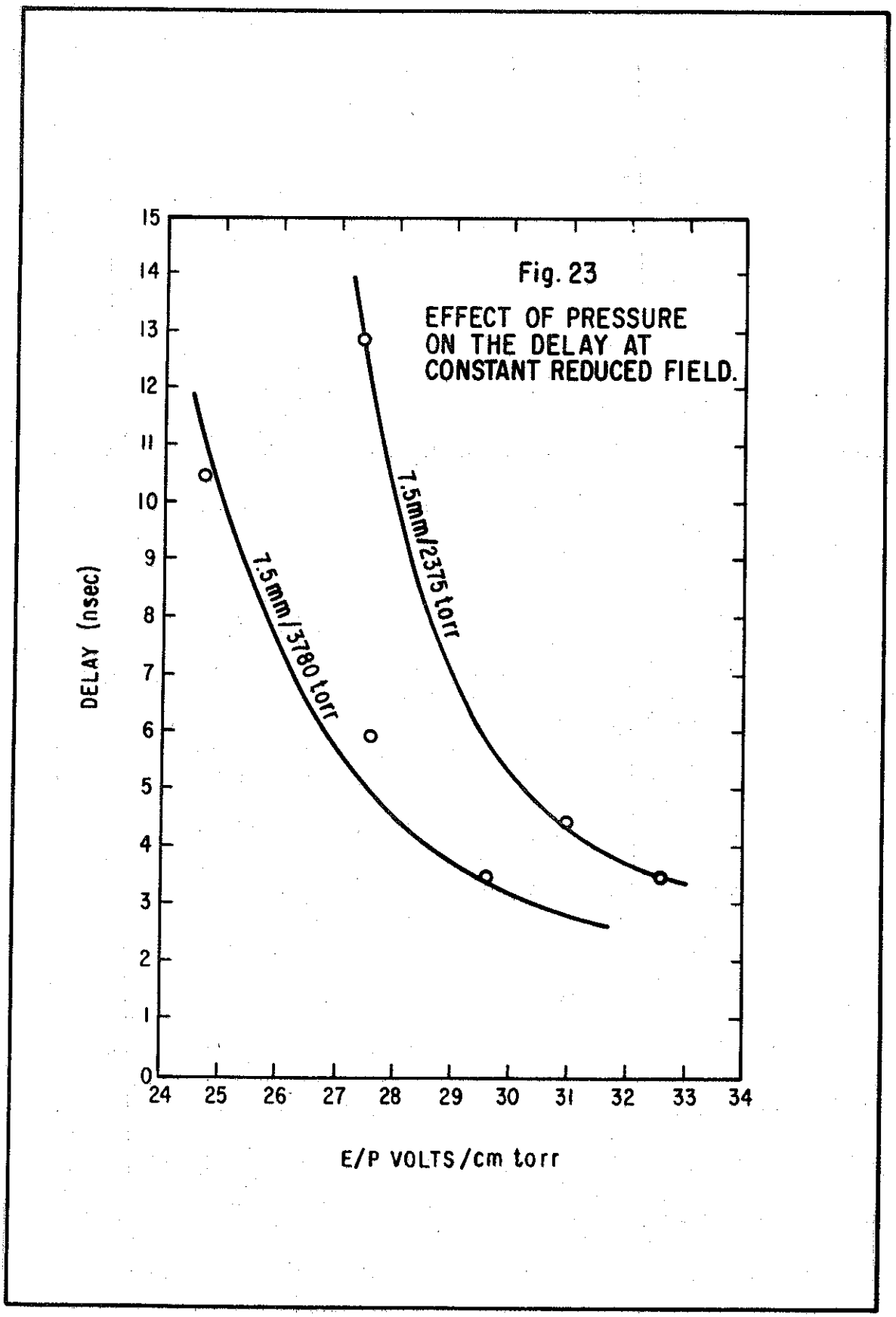
Fig. 23
EFFECT OF PRESSURE ON THE DELAY AT CONSTANT REDUCED FIELD.
7.5mm/2375 torr
7.5mm/3780 torr
DELAY (nsec)
E/P VOLTS/cm torr
0
1
2
3
4
5
6
7
8
9
10
11
12
13
14
15
24
25
26
27
28
29
30
31
32
33
34

Fig. 24. Delay vs. reduced field is plotted in Fig. 24 for two values of gap spacing at nearly the same pressure. The upper curve is for d = 14.9 mm, p = 1880 torr, and V_{SB} = 89.2 kV, and the bottom curve is for d = 11.25 mm, p = 1830 torr, and V_{SB} = 69.2 kV. It is seen that the delay increases with the gap spacing. This indicates that for certain conditions (moderate laser power 150 MW and V_{CH}/V_{SB} about 80% or less) there is definitely a transit effect as opposed to a volume dielectric breakdown effect. That is, the behavior agrees with an ionization growth model (e.g. streamer mechanism) for the breakdown mechanism.

Fig. 25. The pre-breakdown current (Fig. 12) was studied as a function of the reduced field, the laser power, and the electrode material. Figures 25 through 27 are the results of that study. In Fig. 25 the height of the current trace, as recorded by the oscilloscope, is plotted vs. E/p. It is interesting to note that the slope of the current vs. E/p curve is the same as the corresponding portion of the electron drift velocity vs. E/p curve (Fig. 20).

Fig. 26. Here is plotted the height of the current trace vs. laser power. Although data was collected for four electrode materials (tungsten, aluminum, naval brass, and 304 stainless steel), only a composite of these four curves is plotted, because the scatter in the data precluded

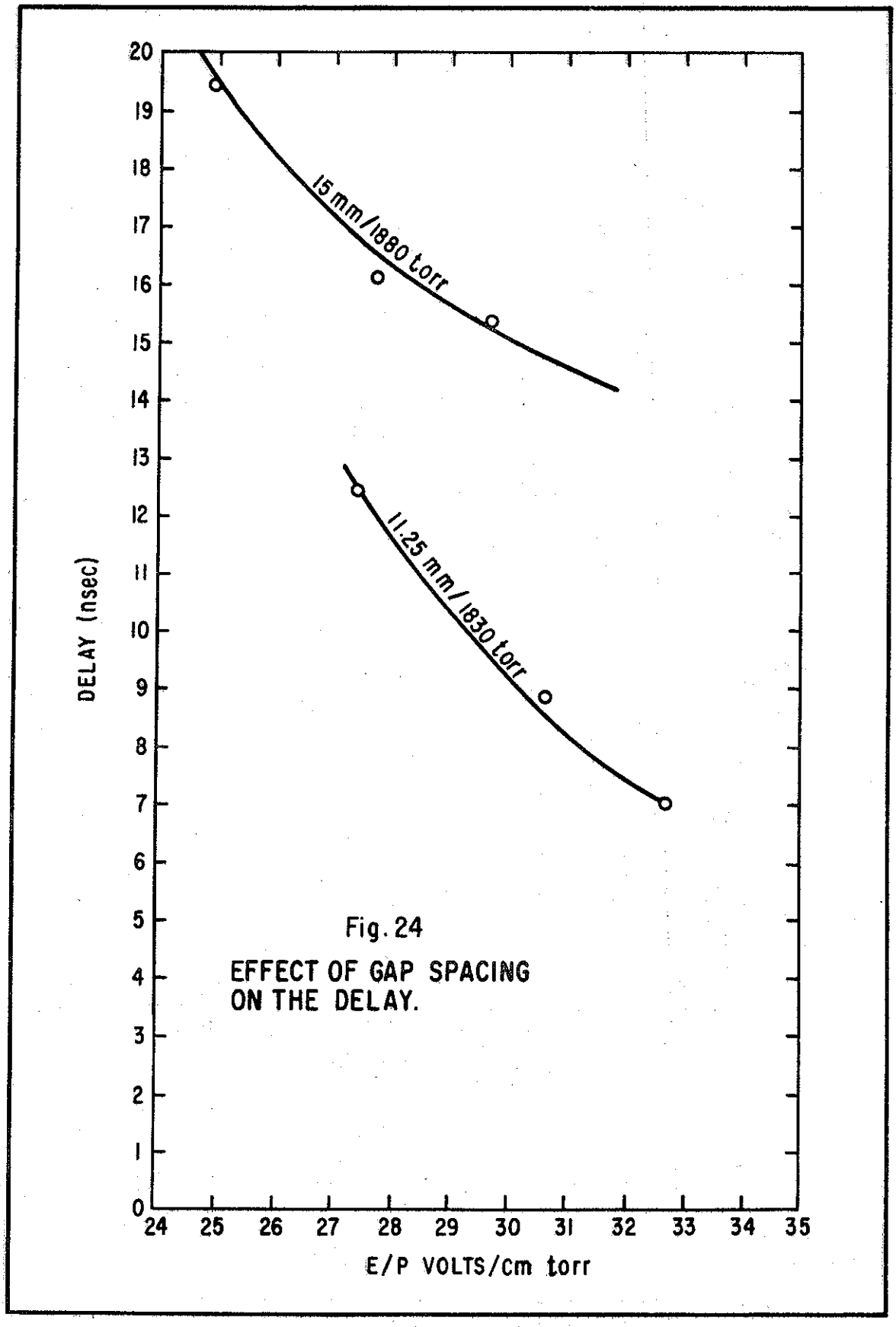

Fig. 24

EFFECT OF GAP SPACING ON THE DELAY.

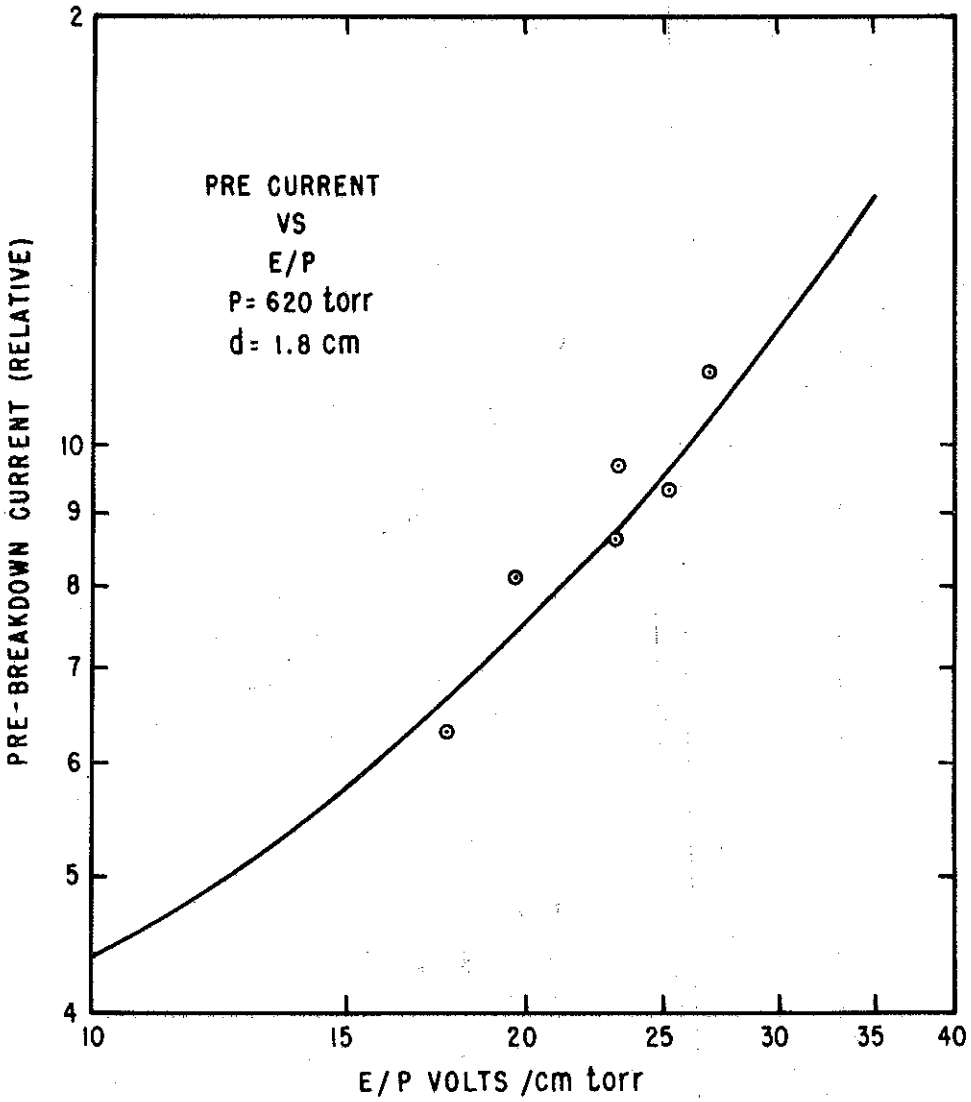

Fig. 25

PRE-BREAKDOWN CURRENT vs REDUCED FIELD

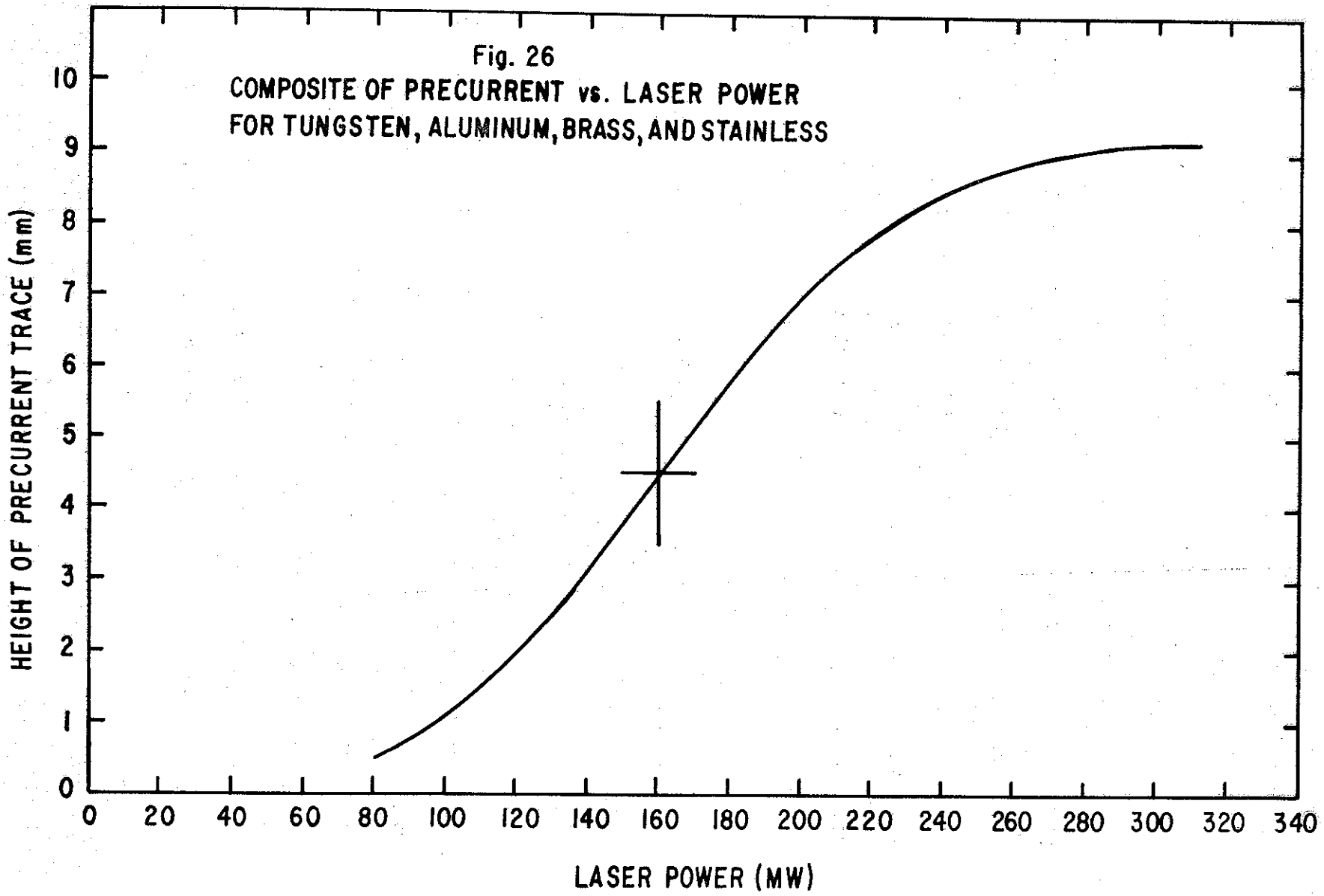
Fig. 26
COMPOSITE OF PRECURRENT vs. LASER POWER
FOR TUNGSTEN, ALUMINUM, BRASS, AND STAINLESS
HEIGHT OF PRECURRENT TRACE (mm)
0
1
2
3
4
5
6
7
8
9
10
0
20
40
60
80
100
120
140
160
180
200
220
240
260
280
300
320
340
LASER POWER (MW)

quantitative determination of the relative magnitude of the current for the various materials.

Fig. 27. An interesting observation is the current trace forms for various materials. Figure 27 makes a comparison of the current form from stainless steel and aluminum. The stainless steel exhibits two peaks, whose height ratio varies with laser power and with reduced field. That is, the first peak increases quicker than the second peak with increasing laser power and reduced field in the gap. The single aluminum peak is typical of the traces for tungsten and brass as well.

Fig. 28. In conjunction with the study of parametric dependencies it was natural to determine if the material of the target electrode would have any bearing on the delay time. Figure 28 shows the results of this inquiry. The laser power was maintained in the 80 to 90 MW range for this investigation, and the self breakdown voltage was kept constant by keeping p and d constant. The order of the curves is not explained.

Fig. 29. The delay vs. $\%V_{SB}$ is plotted for three different laser powers. From upper curve to lower curve the laser powers are: 80-90 MW, 130-165 MW, and 230-280 MW. It should be noted that for quite high laser powers it was possible to trigger the gap with less than 200 nsec delay at 35% V_{SB}.

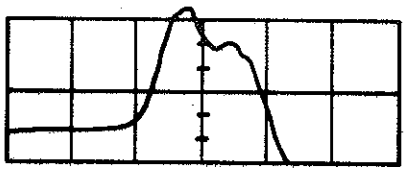

STAINLESS STEEL

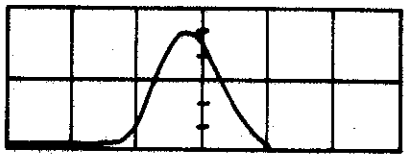

ALUMINUM

Fig. 27

COMPARISON OF THE PRE-BREAKDOWN CURRENT FOR STAINLESS AND ALUMINUM

Fig. 28

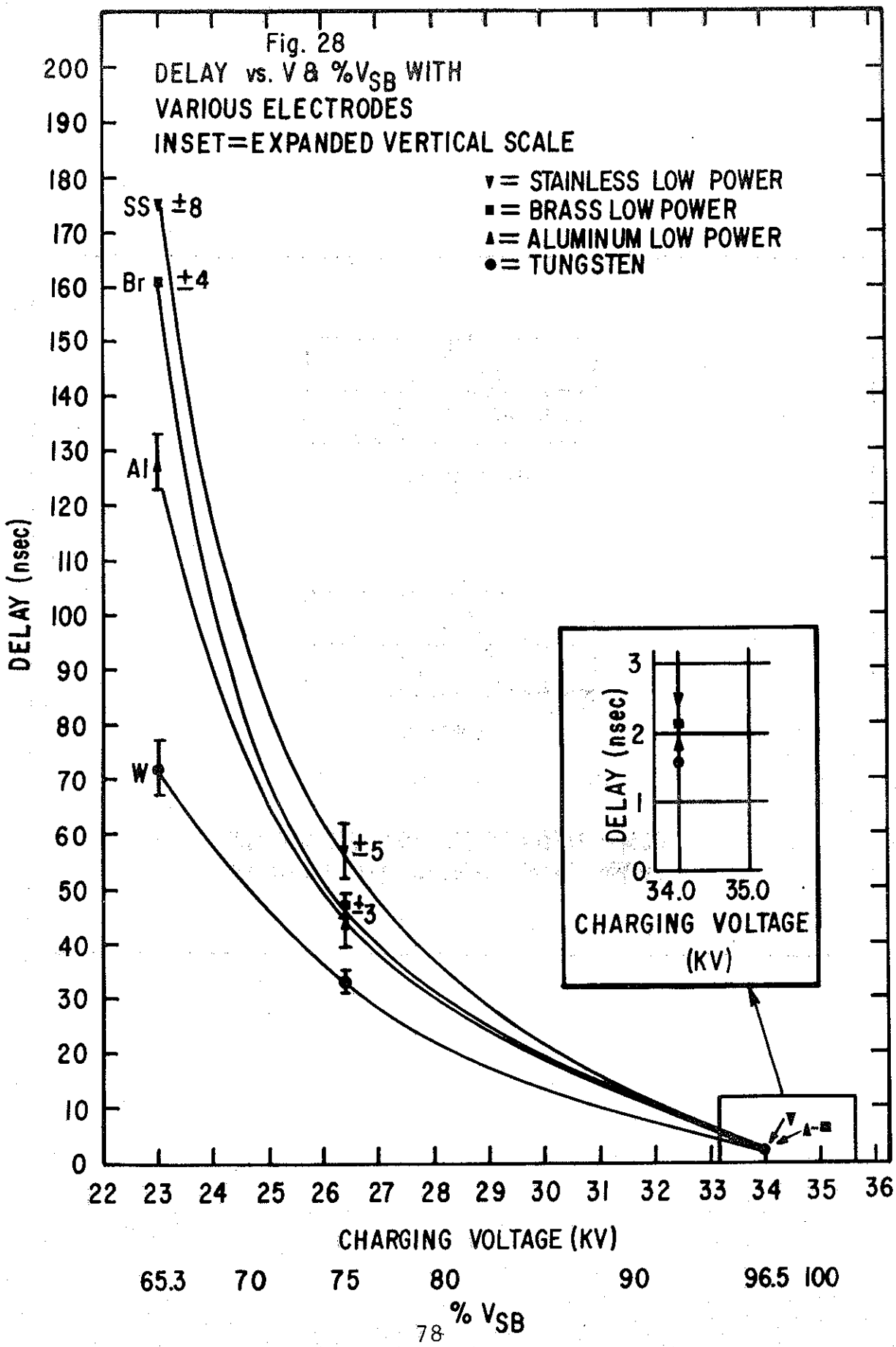
DELAY vs. V & %V_{SB} WITH
VARIOUS ELECTRODES
INSET=EXPANDED VERTICAL SCALE
▼= STAINLESS LOW POWER
■= BRASS LOW POWER
▲= ALUMINUM LOW POWER
●= TUNGSTEN
SS ±8
Br ±4
Al
W
±5
±3
DELAY (nsec)
200
190
180
170
160
150
140
130
120
110
100
90
80
70
60
50
40
30
20
10
0
22 23 24 25 26 27 28 29 30 31 32 33 34 35 36
CHARGING VOLTAGE (KV)
65.3 70 75 80 90 96.5 100
% V_{SB}
DELAY (nsec)
3
2
1
0
34.0 35.0
CHARGING VOLTAGE
(KV)

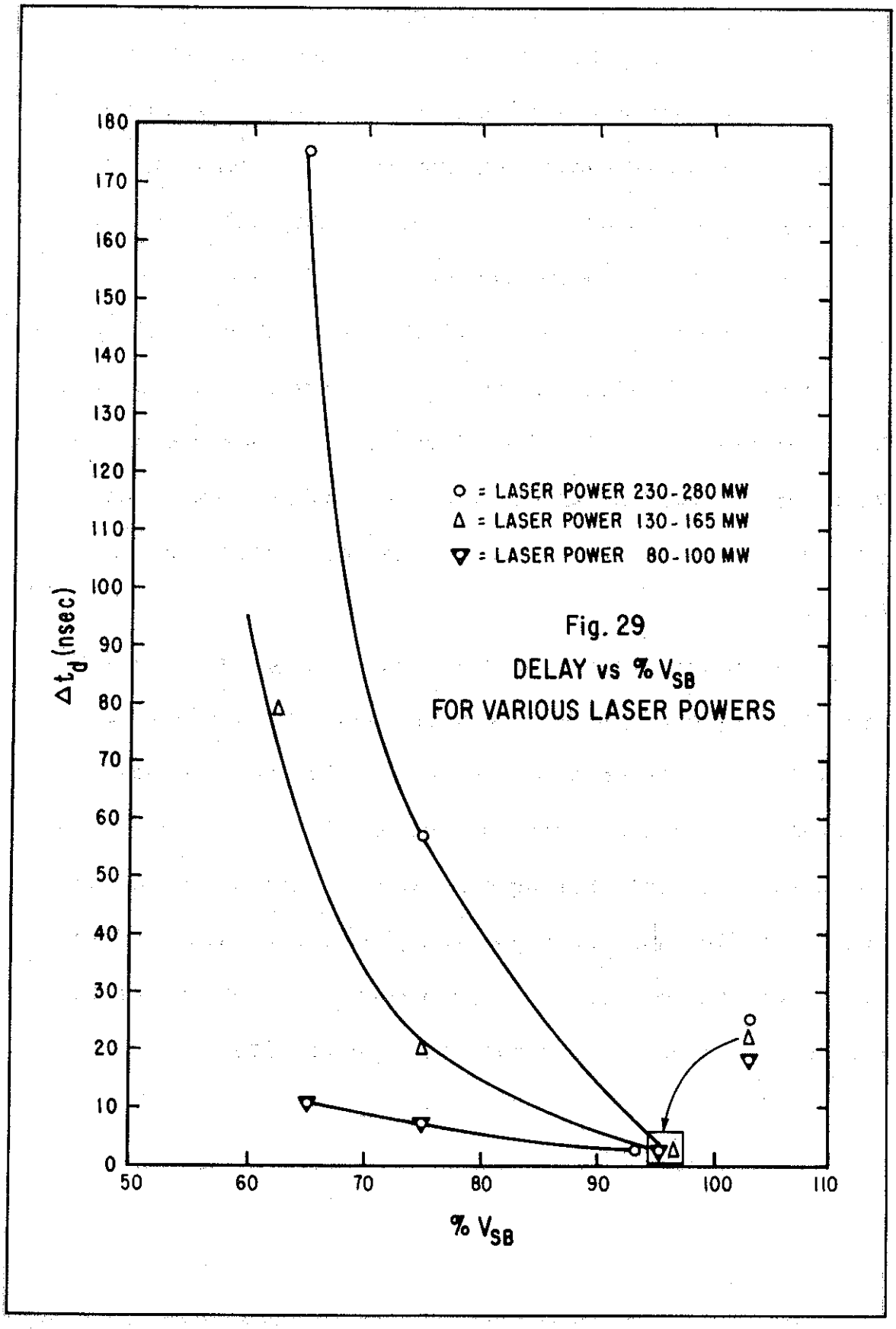

Fig. 29

DELAY vs % V_{SB}

FOR VARIOUS LASER POWERS

Fig. 30. Probably the most important part of this study was the demonstrated ability to trigger systems which had potential differences greater than one megavolt. An extensive research program had been planned, but serious degradation of the column resistors in the Van de Graaff generator limited the reliability of all but a small portion of the data. The data shown in Fig. 30 was obtained with laser powers in the 230-280 MW range. The delay times are very small near V_{SB}, and the correspondingly low jitter ($\pm$ 2 nsec) encourages one to pursue the research on the FX-15.

Preliminary data show that the addition of an electronegative gas has had decided effects on the performance of the switch. At a constant reduced field, delay times increase with the addition of CO_2 and SF_6. However, the improved dielectric strength of the mixture allows higher reduced fields and correspondingly better results. This means that the machine must be operated closer to its self breakdown voltage to achieve the same results.

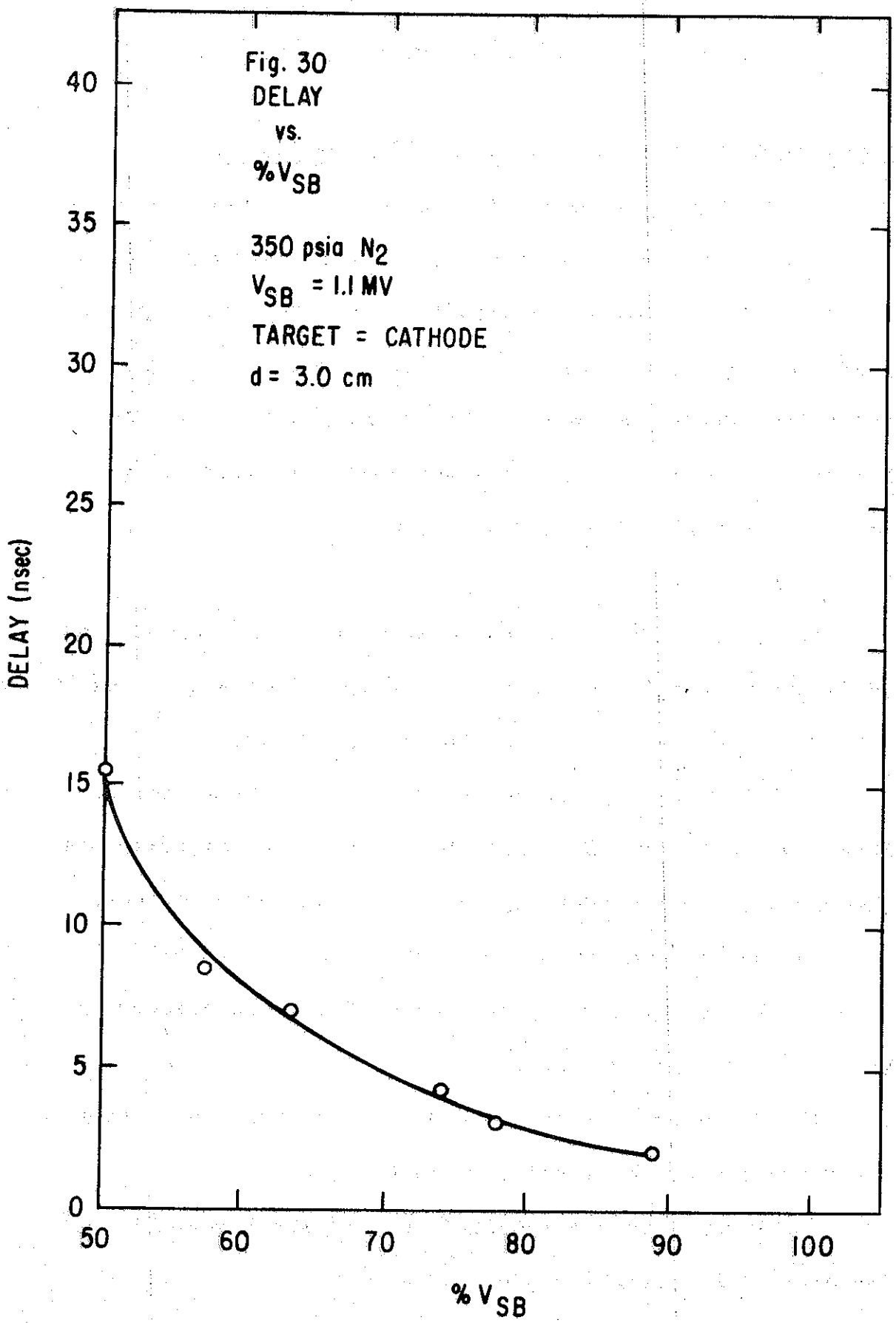
Fig. 30
DELAY
vs.
%V_SB
350 psia N2
V_SB = 1.1 MV
TARGET = CATHODE
d = 3.0 cm
DELAY (nsec)
40
35
30
25
20
15
10
5
0
50
60
70
80
90
100
% V_SB

VI. Conclusions and Recommendations

Comparison of Predicted and Observed Dependencies

The results presented in section V are consistent with the proposed streamer mechanism for laser-induced breakdown (section II). In order to support this contention, the expected behaviors (section II) will be restated and a comparison made with the observed behaviors (section V). The following is a list of the dependencies which would be expected if the streamer theory were applicable to laser-induced breakdown:

(1) If the laser-induced emission from the cathode and anode are nearly the same, shorter delay times should result when the anode is used as the target electrode.

(2) Since α is proportional to E/p, the effect of grounding one electrode should be to decrease the delay when the ungrounded electrode is used as the target electrode.

(3) Delay times should be proportional to $(E/p)^{-9.2}$.

(4) The delay time should be relatively independent of the electron drift velocity.

(5) The switch jitter should be quite small as long as the intensity of the laser beam in the gap is high.

(6) For a constant reduced field, delay times should decrease with increasing pressure.

(7) The delay times should increase as gap spacing is increased.

(8) Delay times should decrease with increasing laser power.

The following is a comparison of observed behavior with the eight points just listed.

(1) Laser-induced emission seems to be independent of the target polarity ((Ref. 7:4963) also confirmed in this study), thus, a comparison of Fig. 16 with Fig. 17 and Fig. 18 with Fig. 19 leads to the expected result. That is, the delay is less when the target electrode is the anode.

(2) A comparison of Fig. 16 with Fig. 18 and Fig. 17 with Fig. 19 reveals that using the ungrounded electrode as the target gives shorter delay times. Thus, from (1) and (2) the best switch performance results from using the ungrounded anode as the target for the laser beam.

(3) It is seen from Figs. 16, 17, 18, and 19 that the predicted value for Δt_d as a function of E/p is in good agreement with observed values. The value of the exponent ranges from -8.27 to -11.6. It is interesting to note that for the case of an ungrounded target, the observed exponent is more positive than the predicted value of -9.2 for both polarities, while for the case of a grounded target, the observed exponent is more negative than -9.2. This would

agree with the observation that the electric field is intensified near the ungrounded electrode.

(4) Figure 20 confirms that the delay times do not depend significantly on the electron drift velocity.

(5) Figures 21, 15, and 11 are needed to support the contention that low jitter results when the laser intensity in the gap is high. In Fig. 21 the jitter varies slowly to about 70% V_{SB}. From Fig. 15 this corresponds to a delay of 35 nsec. From Fig. 11 (50 nsec/div) the intensity of the laser beam is less than a third of the maximum intensity and is rapidly decreasing. Then, for delay times greater than about 35 nsec, the jitter increases rapidly as expected.

(6) Figure 23 reveals that at a constant reduced field, increasing the pressure reduces the delay time. It was mentioned in section II that an empirical fit to the data presented in the paper by Pendleton and Guenther was of the form

$$\Delta t_d = C + (8.5\times 10^4)(1/p) \tag{30}$$

for constant E/p. This agrees with the following form of Eq (13):

$$\Delta t_d = \frac{20 - \ln N_o}{VBp(E/p)^{9.2}} + \frac{d - x_{crit}}{s} \tag{31}$$

That is, at constant E/p

$$\Delta t_d = \frac{20 - \ln N_o}{vB}(1/p) + \frac{d - x_{crit}}{s} \qquad (32)$$

where B is an undetermined constant and v is taken as nearly constant.

(7) From Eq (31)

$$\Delta t_{d1} - \Delta t_{d2} = \frac{d1 - d2}{s} \qquad (33)$$

This assumes E/p is constant and $X_{crit_1} = X_{crit_2}$ for constant E/p. Then, for d_1 = 14.9 mm and d_2 = 11.25 mm, the plot of Δt_d vs. E/p should vary by the constant (0.365/S) nsec. For $S \approx 0.08 cm/sec$ (Ref. 15:181), the difference in Δt_d between d = 14.9 and d = 11.25 mm should be about 4.6 nsec. The observed value of 3-6 nsec agrees within experimental errors.

(8) Figure 29 indicates the dependence of the delay times on laser power. The delay times decrease with increasing laser power. This is explained by the streamer theory on the basis of the increase in N_o (the initial charge carrier concentration) with increasing laser power. From Fig. 26 it is apparent that the pre-breakdown current increases with laser power. It is plausible that the height of the current trace is related to the amount of material removed from the target electrode. In this case, N_o will

increase and Eq (31) gives

$$\Delta t_d(N_o^1) - \Delta t_d(N_o^2) = \frac{\ln N_o^2 - \ln N_o^1}{VBp(E/p)^{9.2}} + \frac{X_{crit}^2 - X_{crit}^1}{s} \qquad (34)$$

Thus, for $N_o^2 > N_o^1$, $\Delta t_d(N_o^1) - \Delta t_d(N_o^2) > 0$. This assumes that

$$\frac{X_{crit}^2 - X_{crit}^1}{s} < \frac{\ln N_o^2 - \ln N_o^1}{VBp(E/p)^{9.2}} \qquad (35)$$

which indeed will be, since the bulk of Δt_d is made up from the latter term in Eq (35). Thus, it is expected that Δt_d will decrease with increasing laser power (particularly at low $\%V_{SB}$) until the saturation value for N_o is reached. The results plotted in Fig. 29 are interesting for two additional reasons: (1) The dependence of the delay time on the reduced field is nearly the same for laser powers of 80 MW and 150 MW. However, the agreement ceases for very short delay times (< 15 or 20 nsec). (2) The dependence of delay time on reduced field for the 250 MW laser power is quite different from the hypothesized behavior (Eq (31)). Thus, it may be conjectured that there are two processes involved in the breakdown mechanism; one, which follows the streamer breakdown theory for delays greater than some minimum value, and another mechanism which depends more strongly on laser power and is much faster. One such process might be the breakdown of the dielectric volume by the laser. Since the

laser is aligned along the path which any subsequent breakdown will follow, a laser power of sufficient magnitude could create a conducting path along which breakdown could rapidly proceed without waiting for avalanche and streamer formation. Certainly, more work needs to be done in this research area.

Applicability of Results to Switch Design

It has been demonstrated that a laser-triggered spark gap can effectively switch voltages up to 90 kV in times less than five nsec with jitter less than one nsec. It is appropriate now to discuss some more of the information obtained during this study.

An important safety feature of a switch, such as the one described here, is that there is no electrical coupling between the switch and the high voltage power supply. The only coupling needed is an optical path to a gap electrode. In systems which have megavolt potential differences, safety cannot be stressed too much, nor the difficulty of triggering the systems with low jitter and low delay.

Although voltage triggering thresholds will vary considerably with switch design and laser power, it should be noted that the atmospheric pressure cell had a triggering threshold of 18-20% V_{SB} for laser power of about 150 MW.

Finally, the results above can be used to predict the feasibility of simultaneously triggering several spark gaps with one laser. One laser pulse could be used to trigger n switches, if partial reflectors were placed in the beam such that $\frac{1}{n - k}$ times the power incident on each reflector were directed into each succeeding gap (k = 0, 1, 2, ..., n-1). This would assure that each gap received the same power density, thereby eliminating the laser power dependence of the delay time. In particular, for n = 2, one 50% reflector would be needed. To take the simplest example, let us suppose that we are required to switch two systems within five nsec. Further assume that they are separated X ft. Since the time of flight of the laser pulse is about 1.02 X nsec, the delay time of the gap closer to the laser must be 1.02 X nsec greater than the delay time of the other gap. This can be prescribed in a number of ways.

The data presented in section V can be used to determine how to vary the system parameters in order to make the time of flight correction. For moderate voltages and laser powers (Figs. 15 and 21), the systems would have to be operated above about 70% V_{SB} to meet the jitter requirement. For a separation not much greater than (35/1.02) ft., a variation in the percent self breakdown voltage to which the gaps are charged would make the time of flight correction.

If the voltages from the two systems were required to be the same, the problem becomes more complex. However, a simple solution would result from increasing V_{SB} of the front gap and charging to a lower percent V_{SB}. This could be done by increasing pd. It would probably be preferable to increase p and leave d constant. The output characteristics would probably be more nearly the same if the gap spacing were held constant.

To see if this is applicable to megavolt switching, let us consider the final graph, Fig. 30.

Megavolt Switching

Using the conclusions just stated, one should be able to construct a switch capable of handling megavolt potential differences and predict the performance of such a switch. Breakdown voltage vs. pressure curves for sphere-sphere spark gaps reveal that at 400 psi in N_2 the reduced field is near 24 volts/cm-torr for breakdown voltages of 1.5 MV when d = 3 cm. This means that α is about 2.07 at 90% V_{SB}, whereas α is about 5.5 at 90% V_{SB} for the atmospheric pressure cell. Then, since Δt_d is proportional to $1/\alpha$, the megavolt switch will have a slower response. To offset this, N_o could be increased by increasing the laser power. In addition, a lens with a longer focal length would allow

the laser to produce greater ionization throughout the volume, which would reduce jitter and increase the avalanche and streamer propagation velocities. Both of these changes were made to obtain the results shown in Fig. 30. It is seen in Fig. 30 that the delay times vary slowly with $\%V_{SB}$. This can be compared with the results in Fig. 29 for high laser power. The laser power used in obtaining the curve in Fig. 30 and the lowest curve in Fig. 29 were in the 230-280 MW range.

The conclusion, then, is that it is possible to switch megavolt systems with less than three nsec delay times. The risetime of the voltage pulse upon breakdown was two nsec.

Each data point in Fig. 30 represents from three to five shots. No detailed study of the jitter was made because of the degradation of the column resistors in the Van de Graaff generator. However, an outside limit may be placed on the switch jitter from the spread in the data.

The data spread for Fig. 30 was about $\pm$ 3 nsec when the delay was 15 nsec, and about $\pm$ 1 nsec when the delay was less than five nsec. The highest voltage which was triggered with this system was 1.1 MV, with less than 10 nsec delay for V_{SB} = 1.5 MV. With a more stable power supply there should be no difficulty in obtaining triggering delay times of less than five nsec and switch jitters of less than one nsec.

Recommendations for Further Research

Several questions have been left unanswered that future research could resolve. The following recommendations are of a basic research nature: (1) investigate the temporal growth of ionization with a high speed streak camera, (2) investigate the switch jitter as a function of laser power more thoroughly, (3) study the resistive and inductive phases of the breakdown, and (4) study the effect of dielectric fill in more detail.

From an engineering standpoint it would be useful to: (1) demonstrate the feasibility of synchronously switching more than two gaps, (2) extend the dielectric study to include solids and liquids, (3) study the possibility of repetitively switching spark gaps with high repetition-rate lasers, and (4) develop a method of producing multiple breakdown channels within a single gap in order to reduce inductance.

Bibliography

1. Andreev, S. I., and B. M. Sokolov. "Formation of a Spark Channel in Air." Soviet Physics-Technical Physics, 10:1003-1005 (January 1966).

2. Barbini, S. "Coaxial Laser-Triggered Gap Study." Conference on Controlled Thermonuclear Reactions, Frascatti, Italy (1966).

3. Cobb, J. K., and J. J. Muray. "Laser Beam-Induced Electron and Ion Emission from Metal Foils." British Journal of Applied Physics, 16:271-273 (1965).

4. Cobine, James Dillon. Gaseous Conductors. Dover Publications, Inc., New York (1958).

5. David, C., P. V. Avizonis, H. Weichel, C. Bruce, and K. O. Pyatt. "Density and Temperature of a Laser Induced Plasma." IEEE Journal of Quantum Electronics, QE-2:493-499 (September 1966).

6. Deutsch, F. Development of a Laser-Triggered Spark Gap Feasibility Study. MPS, Cern, Switzerland (10 February 1967).

7. Ehler, A. W. "Plasma Formed by a Laser Pulse on a Tungsten Target." Journal of Applied Physics, 37: 4962-4966 (December 1966).

8. Gilmour, A. S., R. E. Bliss, and R. J. Clark. Laser-Triggered Switch Study. Air Force, Cato Show Printing Company (17 November 1966).

9. Gold, A., and H. B. Bebb. Physical Review Letters, 14:60 (1965).

10. Iannuzzi, M., and R. Williamson. "Effects of Absorption of Laser Radiation on Metals." Il Nuovo Cimento, XXXVI:2410-2414 (16 April 1965).

11. Isenor, N. R. "Effect of Background Gas on Laser-Induced Electron Emission from Metal Surfaces." Journal of Applied Physics, 36:316-317 (January 1965).

12. Jackson, John David. Classical Electrodynamics. John Wiley and Sons, Inc., New York (1963).

13. Knecht, Walter L. "Initial Energies of Laser-Induced Electron Emission From W." Applied Physics Letters, 6:99-100 (15 March 1965).

14. Martin, Charles. AWRE, Private Communication with A. H. Guenther.

15. Meek, J. M., and J. D. Craggs. Electrical Breakdown of Gases. Oxford at the Clarendon Press (1953).

16. Meyerand, R. G., Jr., and Alan F. Haught. "Optical-Energy Absorption and High-Density Plasma Production." Physical Review Letters, 13:7-9 (6 July 1964).

17. Pendleton, W. K., and A. H. Guenther. "Investigation of a Laser Triggered Spark Gap." The Review of Scientific Instruments, 36:1546-1550 (November 1965).

18. Peressini, Eugene R. "Field Emission from Atoms in Intense Optical Fields." Physics of Quantum Electronics Conference Proceedings, P. L. Kelley, B. Lax, and P. E. Tannenwald, Editors, 499-508, McGraw-Hill, New York (1966).

19. Raether, Heinz. Electron Avalanches and Breakdown in Gases. Butterworths, Washington (1964).

20. Ready, J. F. "Mechanism of Electron Emission Produced by a Giant-Pulse Laser." The Physical Review, 137: A620-A623 (18 January 1965).

21. Verber, C. M., and A. H. Adelman. "Laser-Induced Thermionic Emission From Tantalum." Journal of Applied Physics, 36:1522-1525 (May 1965).

22. von Engel, Alfred. Ionized Gases. Oxford at the Clarendon Press (1965).

23. Weichel, Hugo, and P. V. Avizonis. "Expansion Rates of the Luminous Front of a Laser-Produced Plasma." Applied Physics Letters, 9:334-337 (1 November 1966).

Appendix A

Error Analysis

It is always interesting to make an analysis of the errors that are introduced into reported data. A report of data without a corresponding report on the reliability of the data places a burden on other investigators wishing to reproduce the data. Often, when the physical processes involved are not well understood, it is necessary to analyze the data with respect to the empirically derived dependencies. The research reported in this study falls into this category.

The measurement of interest in this study was the time delay between the arrival of the laser pulse at the gap and the breakdown of the gap. Two types of uncertainties are associated with the determination of the delay time: (1) uncertainties associated with measurements such as the distance from the laser to the gap, the distance from the gap to the oscilloscope, and the distance between the events as recorded by the trace photographs, and (2) uncertainties introduced by the variation of the system parameters such as charging voltage, laser power, and dielectric composition and pressure. The first type of uncertainty is relatively

easy to deal with. Every measurement has an error associated with it, which is determined by the instrument used to make the measurement. It is also evident that such errors will have a bearing only on the absolute value of the delay time. That is, if the process being investigated were exactly reproducible and the total errors of type (1) amounted to 0.5 nsec, such that a delay of 5 nsec recorded as 4.5 nsec, then the delay would be recorded as 4.5 nsec every time the same process occurred. This assumes, of course, that the data is recorded with any desired precision. If the conditions just listed were true, the error analysis would be short and easy to make, however, the initial conditions of the equipment were hard to prescribe, and the data could not be recorded with infinite precision. These uncertainties lead to a variation in the reproducibility of the process, which has been termed switch jitter. The task in this error analysis, then, is to account for as much of the switch jitter as possible.

The system parameters which have a bearing on the delay time are: the electric field in the gap, the composition and pressure of the gas dielectric, the percentage of the self breakdown voltage to which the gap is charged, and the output power of the laser. Other parameters influence the delay time (e.g. gap polarity and the location and size of

the laser focus (Ref. 17:1547)), but are not considered in the error analysis since they were easy to maintain. Additional errors were introduced by the way in which the data was recorded--these errors will be considered first.

It was reported in section III that the uncertainty in reading the oscilloscope traces was ± 0.08 mm in the first 5 mm and ± 0.07 mm after 2 cm of sweep. The following uncertainties in the event times are the result: (1) at 20 nsec/cm the uncertainties are ± 0.25 nsec and ± 0.25 nsec, for a total uncertainty in the signal delay of ± 0.5 nsec, (2) at 50 nsec/cm the uncertainties are ± 1.5 nsec and ± 0.7 nsec, for a total uncertainty of ± 2.2 nsec, (3) at 100 nsec/cm the uncertainties are ± 3 nsec and ± 1 nsec, for a total uncertainty of ± 4 nsec. The ranges of delay measured on each sweep rate setting were: 0 to 35 nsec on 20 nsec/cm, 35 to 270 nsec on 50 nsec/cm, and greater than 270 nsec on 100 nsec/cm. The error just considered has the effect of reducing the abruptness of the jitter vs. $\%V_{SB}$ curve (Fig. 21) at 67-70% V_{SB}. However, the correction is not enough to reverse the author's claim of low jitter at intense radiation levels, but rather strengthens the claim, since the jitter increases more slowly near the last 1/3 of the laser pulse.

To investigate the parametric dependence of jitter, recall Eq (31):

$$\Delta t_d = \frac{20 - \ln N_o}{VBp(E/p)^{9.2}} + \frac{d - x_{crit}}{s} \tag{31}$$

From Fig. 16 the actual dependence is

$$\Delta t_d = A_1 (E/p)^{-8.27} \tag{26}$$

so that if v is taken as constant, we obtain for Eq (31):

$$\Delta t_d = \frac{20 - \ln N_o}{C\, p(E/p)^{8.27}} + \frac{d - x_{crit}}{s} \tag{36}$$

where C is a constant. Taking finite differences

$$j = 7.27 \Delta t_d \frac{\delta p}{p} + 8.27 \Delta t_d \frac{\delta U_g}{U_g} + L \tag{37}$$

where j is the jitter, Ug is the gap potential, and L is an undetermined variation caused by the fluctuation of the laser power.

The term $\delta U_g / U_g$ in Eq (37) lies between 0.005, at Ug = 15 kV, and 0.01 at Ug = 30 kV. The term $\delta p / p$ was a measure of the fluctuation in ambient air pressure and had a magnitude of 0.0008. Then Eq (37) becomes

$$j = 0.006 \Delta t_d + 0.0827 \Delta t_d + L \tag{38}$$

for Ug between about 25 and 30 kV and

$$j = 0.006 \Delta t_d + 0.0414 \Delta t_d + L \tag{39}$$

for Ug between about 10 and 25 kV. This gives typical values for jitter of ± 9.4 nsec, for $\Delta t_d = 200 nsec$, and ± 2.8 nsec, for $\Delta t_d = 60 nsec$. These compare with ± 21 nsec, for $\Delta t_d = 200 nsec$, and ± 7 nsec, for $\Delta t_d = 60 nsec$—Figs. 15 and 21. It is apparent that both the computed values are less than half the observed value. For 70% V_{SB} or greater, the predicted jitter agrees with the observed jitter to within 10%. However, the dependence on laser power has not been accounted for and must remain so at this writing. A check of Fig. 28 reveals that at lower laser power the jitter is lower. This particular variation of the delay time must be due to the $\ln N_o$ term in Eq (31). If it is true that the pre-breakdown current is proportional to the number of charge carriers which the laser beam produces, Fig. 26 reveals that N_o varies nearly linearly with laser power. Then, as a first approximation we could write

$$\ln N_o = \ln gM \tag{40}$$

where M is the laser power and g is a constant. The jitter introduced by the laser power could then be approximated from Eq (31) as

$$\delta(\Delta t_d) \approx \frac{-\delta M}{M} \frac{1}{cp(E/p)^{8.3}} \tag{41}$$

which leads to

$$j_M = \left[\Delta t_d - \frac{20}{cp(E/p)^{8.3}}\right] \frac{\delta M}{M \ln g M} \tag{42}$$

Twenty shots were taken at laser powers of 80 and 150 MW with the following results:

$$\left[\frac{\delta M}{M}\right]_{80} = 0.17 \tag{43}$$

and

$$\left[\frac{\delta M}{M}\right]_{150} = 0.135 \tag{44}$$

Unless g decreases with laser power (the reverse seems true from Fig. 26) the jitter caused by the variation in laser power should diminish as power increases. This is contrary to preliminary observations, and further verification of this anomalous behavior seems necessary.